

1 **Main Manuscript for**

2 **NeurOne: High-performance Motor Unit-Computer Interface for the**  
3 **Paralyzed**

4

5 **Authors:**

6 Dominik I. Braun<sup>1</sup>, Daniela Souza de Oliveira<sup>1</sup>, Patricia Bayer<sup>1</sup>, Matthias Ponfick<sup>2</sup>, Thomas Mehari  
7 Kinfe<sup>3</sup>, Alessandro Del Vecchio<sup>1</sup>

8 **Author affiliation:**

9 <sup>1</sup> Department Artificial Intelligence in Biomedical Engineering, Friedrich-Alexander-Universität  
10 Erlangen-Nürnberg, 91052 Erlangen, Germany.

11 <sup>2</sup> Querschnittszentrum Rummelsberg, Krankenhaus Rummelsberg GmbH, 90592  
12 Schwarzenbruck, Germany.

13 <sup>3</sup> Department Neurological Surgery, Friedrich-Alexander-Universität Erlangen-Nürnberg, 91054  
14 Erlangen, Germany.

15 **Corresponding author:** Alessandro Del Vecchio

16 **Email:** [alessandro.del.vecchio@fau.de](mailto:alessandro.del.vecchio@fau.de)

17 **Competing Interest Statement:** Disclose any competing interests here.

18 **This PDF file includes:**

19 Main Text  
20 Figures 1 to 6  
21 Tables 1 to 1  
22

## 23 **Abstract**

24 We have recently demonstrated that humans with motor-and-sensory complete cervical spinal cord  
25 injury (SCI) can modulate the activity of spared motor neurons that control the movements of  
26 paralyzed muscles. These motor neurons still receive highly functional cortical inputs that  
27 proportionally control flexion and extension movements of the paralyzed hand digits. In this study,  
28 we report a series of longitudinal experiments in which subjects with motor complete SCI received  
29 motor unit feedback from NeurOne. NeurOne is a software that realizes super-fast digitalization of  
30 motor neuron spiking activity (32 frames/s) and control of these neural ensembles through a  
31 physiological motor unit twitch model that enables intuitive brain-computer interactions closely  
32 matching the voluntary force modulation of healthy hand digits. We asked the subjects (n=3, 3-4  
33 laboratory visits) to match a target displayed on a monitor through a cursor that was controlled by  
34 the modulation of the recruitment and rate coding of the spared motor units using a motor unit  
35 twitch model. The attempted movements of the paralyzed hands involved grasping and hand digit  
36 extension/flexion. The target cursor was scaled in a way that the subjects could increase or  
37 decrease feedback by either recruiting or derecruiting motor units, or by modulating the  
38 instantaneous discharge rate. The subjects learned to control the motor unit output with high levels  
39 of accuracy across different target intensities up to the maximal achievable discharge rate. Indeed,  
40 the high-performance motor output was surprisingly stable in a similar way as healthy subjects  
41 modulated the muscle force output recorded by a dynamometer. Therefore, NeurOne enables  
42 tetraplegic individuals an intuitive control of the paralyzed muscles through a digital neuromuscular  
43 system.

## 44 **Significance Statement**

45 Our study demonstrates the remarkable ability of individuals with complete cervical spinal cord  
46 injuries to modulate spared motor neurons and control paralyzed muscles. Utilizing NeurOne, a  
47 software, we enabled intuitive brain-computer interactions by digitalizing motor neuron spiking  
48 activity and employing a motor unit twitch model. Through this interface, tetraplegic individuals  
49 achieved high levels of accuracy and proportional control which closely resembled motor function  
50 in intact humans. NeurOne provides a promising digital neuromuscular interface, empowering  
51 individuals to control assistive devices super-fast and intuitive. This study signifies an important  
52 advancement in enhancing motor function and improving the quality of life for those with spinal cord  
53 injuries.

## 54 55 **Main Text**

### 56 57 **Introduction**

58 The human hand is a remarkable structure with a complex set of movements that allow us to  
59 perform various tasks with ease. The control of hand movements is governed by a network of neural  
60 pathways that originate from the brain and the spinal cord and involve upper and lower motor  
61 neurons that control muscle forces. Electromyography (EMG) measures the electrical activity  
62 generated by muscle fibers during muscle contraction, with surface EMG (sEMG) being a non-  
63 invasive technique that can provide a comprehensive picture of motor unit activity across space  
64 and time (1, 2). Recent advancements in sEMG, particularly high-density sEMG (HD-sEMG), have  
65 allowed for accurate extraction of individual motor units using techniques such as convolutive  
66 kernel compensation (CKC) and fast independent component analysis (FastICA) (3–9). The  
67 characteristics of motor units have been investigated in both isometric and dynamic movements of  
68 the hand (4, 8, 10–13), with some studies showing the identification of unique motor units specific  
69 to certain movement patterns (14). Real-time decomposition of sEMG signals into motor unit firings,  
70 also known as online decomposition, has been successfully applied using convolutive blind source  
71 separation (BSS) techniques and gated recurrent units (GRU) (15–19).

72 For individuals with neuromuscular diseases or paralysis resulting in hand immobility, visual  
73 feedback of their hand movement intention is not possible. However, real-time identification of the  
74 firing motor unit activity from HD-sEMG signals might provide a solution for this lack of control. Ting  
75 et al. demonstrated that an individual with motor complete SCI still had functional motor neurons

76 that can be extracted through the decomposition of HD-sEMG signals (20, 21). Similarly, we found  
77 unique motor units in eight motor complete SCI patients with a lesion at level C5-C6 who attempted  
78 predetermined hand movements (22). These patients were also able to track a visual cue on a  
79 monitor by modulating the discharge rate of the identified motor units in real-time (22).

80 Here, we present NeurOne, a software that provides paralyzed individuals with fast and accurate  
81 motor neuron feedback. As motor neurons represent the last neural code of movement that is then  
82 translated into muscle force, this interface enables direct control of the movements that were once  
83 paralyzed without the need of remapping to new motor dimensions. The software uses an online  
84 decomposition method that extracts motor unit action potentials from HD-sEMG signals through  
85 convolutive BSS embedded with a super-fast digitalization of the spiking activity (>30Hz), and a  
86 motor unit twitch model with physiological delay for the user-in-the-loop computer interaction.  
87 Although there are algorithms already capable of identifying the motor unit activity (15, 23, 24),  
88 these have very low time resolutions (<10 Hz) and do not include a realistic motor unit twitch model  
89 and therefore are not intuitive. More importantly, these previous algorithms have not been  
90 developed for paralyzed individuals which requires software with high user-in-the-loop capabilities,  
91 as demonstrated in the paragraphs below. The software is used by asking individuals with  
92 paralyzed hands to attempt various dynamic hand movements guided by a virtual hand to ensure  
93 that the HD-sEMG signals are synchronized. The HD-sEMG signals (128 electrodes) are measured  
94 from the surface of the forearm, and the extracted motor unit action potentials are used to decode  
95 the signals at a rate of 32 Hz, providing real-time feedback on task-related motor unit firings. After  
96 identifying the motor unit spike trains, NeurOne generates a task-related cumulative motor unit  
97 spike train, which is convolved with a physiological optimized motor unit twitch model to provide  
98 smooth feedback. To evaluate the accuracy of NeurOne, participants are asked to follow a  
99 requested trajectory that involves ramps with different activation levels. The accuracy is then  
100 calculated using the Pearson correlation coefficient (PCC)  $r$  and the root-mean-square error  $RMSE$   
101 normalized to the respective activation level. We evaluated the accuracy on a subset of three  
102 patients with chronic cervical SCI who visited the laboratory over the course of up to two months.  
103 After just one day of training sessions, these patients could reliably track a visual cue on a monitor  
104 at a large range of neural activation levels. The feedback provided by NeurOne reached a  
105 coefficient of variation  $cv$  similar to the variability of the measured force in healthy subjects during  
106 the plateaus of ramp trajectories in different hand and lower limb muscles.

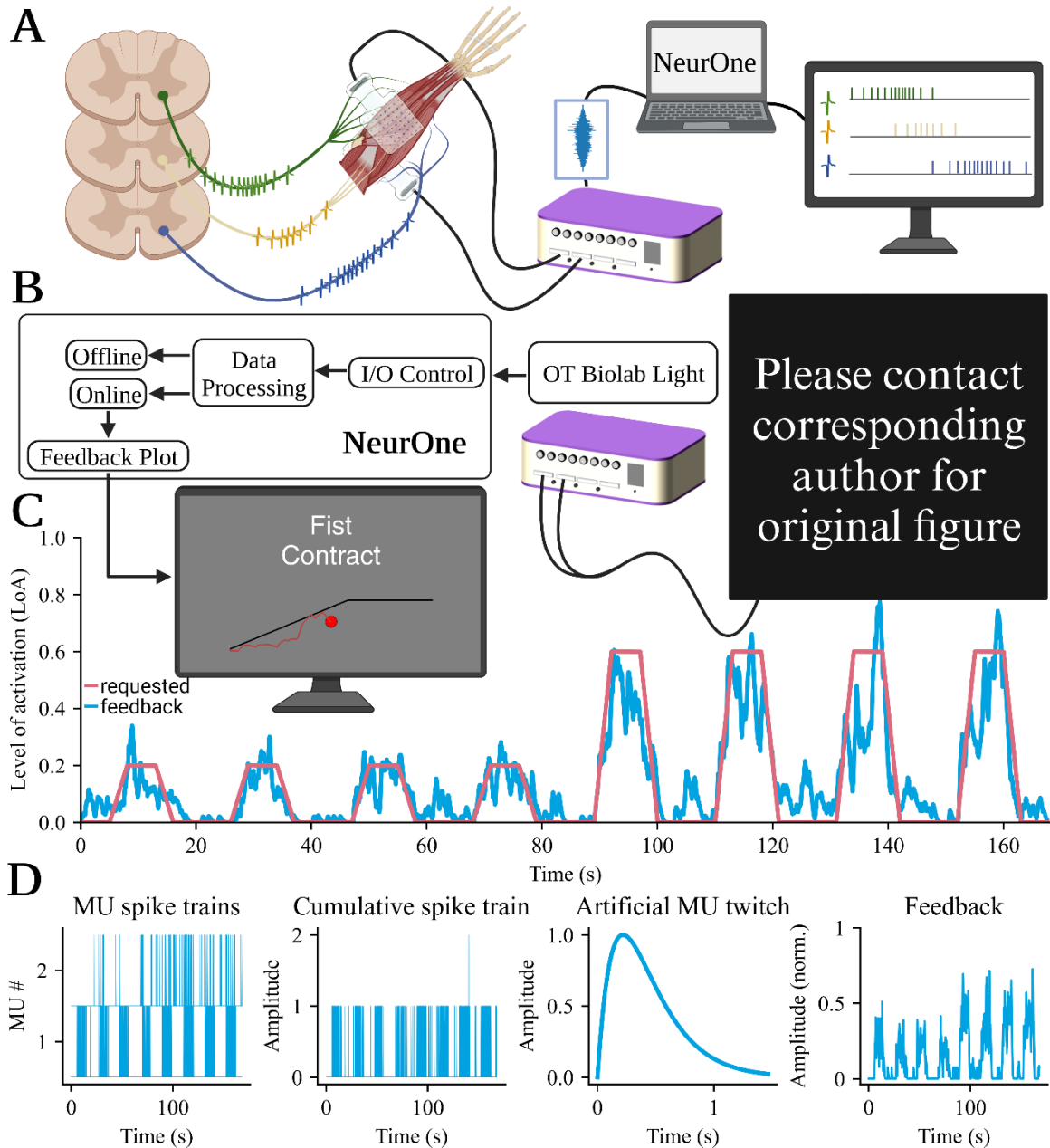
107 This innovative software offers a potential solution for individuals with paralysis resulting in hand  
108 immobility, providing them with a new level of control in a minimally invasive way. By allowing  
109 paralyzed individuals to use their remaining motor neurons to control their hand movements  
110 through real-time feedback, NeurOne offers a promising avenue for restoring mobility and  
111 independence.

## 112 **Results**

### 113 *Interfacing Motor Units in SCI*

114 We present a novel technique for non-invasive interfacing of the spinal motor neurons in individuals  
115 with motor and sensor-complete cervical SCI. Our method involves the application of BSS on HD-  
116 sEMG recordings to identify individual motor unit firings in real-time and rendering of the neural  
117 activity through a super-fast decomposition and integration of visuomotor feedback through a motor  
118 unit twitch model. The HD-sEMG electrodes are placed on the extensor digitorum and flexor  
119 digitorum superficialis muscle in the forearm to measure muscle activity, as these muscles are  
120 involved in almost all digit movements of the human hand.

121 We integrated our non-invasive motor unit interface based on convolutive BSS into our software  
122 NeurOne, which allows users to interact with physiological latency with the spared neural activity



Please contact  
corresponding  
author for  
original figure

123 **Figure 1.** Overview of the experimental protocol used in individuals with spinal cord injury (SCI). A) We recorded high-density surface electromyographic (HD-sEMG) signals from the forearms of participants with SCI by applying two electrode  
124 grids with 64 channels each on top of the extensor digitorum and flexor digitorum superficialis muscles. These signals  
125 represent an estimate of the activity of the spared motor units that controls hand movements. We used a multichannel  
126 amplifier to collect the HD-sEMG signals and stream them to a computer that runs NeurOne. NeurOne decomposes the  
127 streamed HD-sEMG signals into individual motor unit firings. B) NeurOne used in the study where either offline or online  
128 decomposition on the acquired HD-sEMG signals from the forearm of the participant was performed. By attempting specific  
129 hand movements such as power grasp or pinch, the participants were instructed to follow a trajectory displayed on a screen  
130 during the online session. The neural feedback for the hand movements was calculated by NeurOne and displayed to the  
131 participant through a cursor on a monitor. C) An online session of participant S3, where the participant followed a requested  
132 trajectory (red line) by modulating the motor unit activity (blue line). The participants attempted to control the movement of  
133 the paralyzed hand, and the feedback from NeurOne allowed real-time adjustments of the spared motor commands to  
134 achieve the desired trajectory. D) NeurOne calculates the feedback by convolving the task-related cumulative motor unit  
135

136 spike train decomposed by NeurOne with a physiological optimized motor unit twitch model. This approach provides smooth  
137 and super-fast feedback that helped the participants adjusting the movements in real-time.

138  $(32 \frac{\text{frames}}{\text{s}})$ . This latency enables visuomotor feedback without the perception of any delay for the  
139 user. Figure 1 shows the overview of NeurOne describing the pipeline for decoding motor unit  
140 spiking activity and the closed-loop user interaction display where SCI subjects followed predefined  
141 trajectories with a cursor controlled by their smoothed motor neuron spiking activity during hand  
142 digit movements. NeurOne decoded individual motor unit firings in real-time by decomposing the  
143 measured HD-sEMG signals on the forearm (Figure 1A).

144 We performed longitudinal tests on three individuals diagnosed with complete SCI affecting motor  
145 and sensory functions in four separate sessions, over a period of two weeks, except for participant  
146 2, who could only complete three sessions. For this participant, the first two sessions occurred  
147 within a week, while the final session took place two months later. The subjects present no  
148 movement in their hand, and they have no visible feedback when asked to attempt tasks. Here, we  
149 demonstrate that the feedback provided by NeurOne can bypass the injury and allow SCI  
150 individuals to reliably interact with a computer by attempting hand movements.

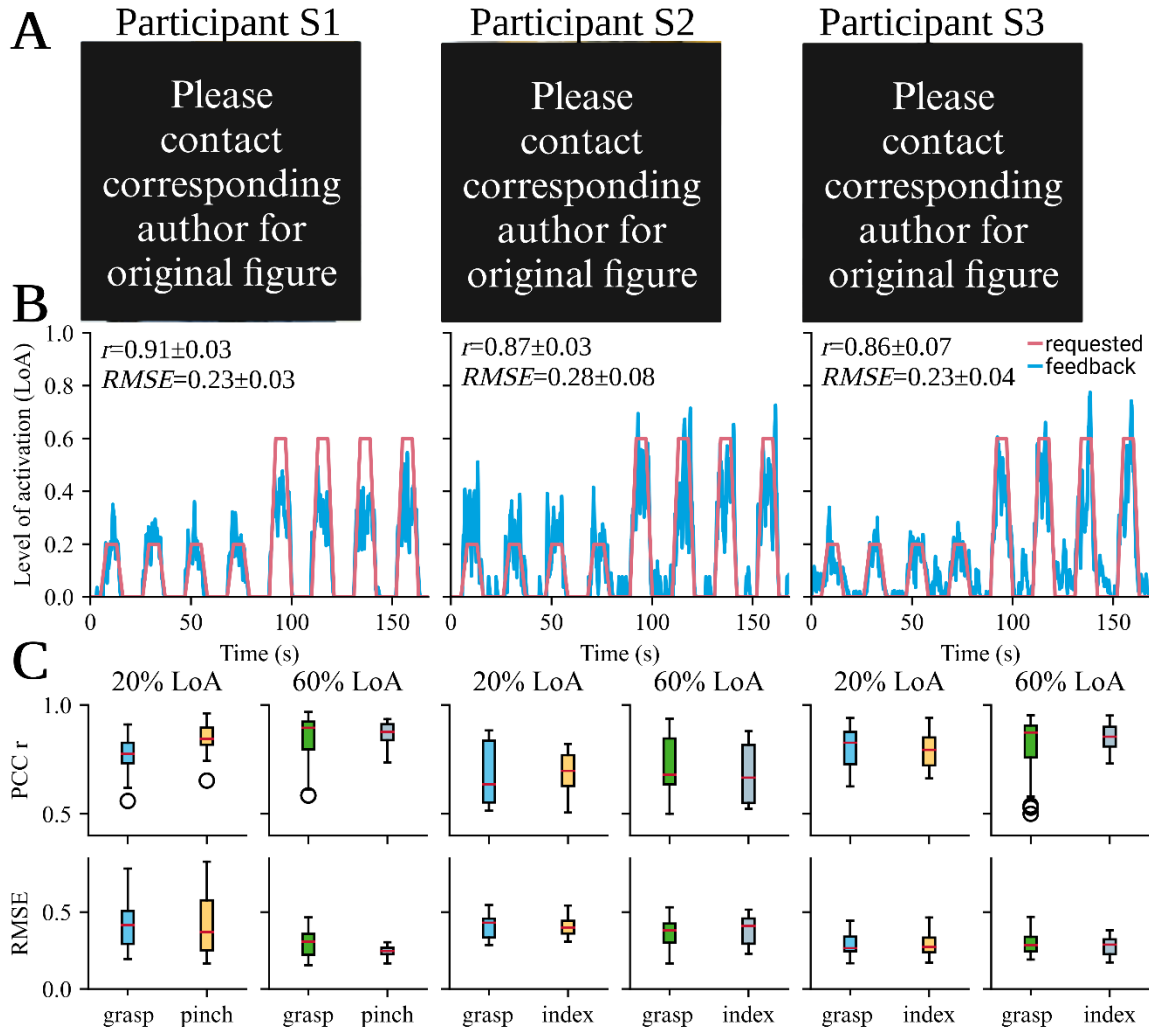
151 In each session, we performed a short warm-up in which the subjects were asked to follow a virtual  
152 hand displayed on a screen. Subsequently, we recorded 20 seconds of contractions to find the  
153 separation matrices (the motor unit filters), which are used in the BSS iterative process to calculate  
154 the source signals from the observations and from which the motor unit action potentials are  
155 calculated through spike-triggered-averaging. During the online part, we applied these filters such  
156 that the subjects could follow the requested trajectory with high accuracy (Fig. 2B). One online  
157 session of participant S6 is displayed in Figure 1C. The feedback is represented through the blue  
158 line while the requested trajectory is shown in red.

159 To calculate the feedback, i.e., the smoothed motor neuron spiking activity, we identified all motor  
160 unit spike trains involved in an individual hand digit movement, summed the spike trains across all  
161 motor units, and convolved the firing activity (series of zeros and ones) with an artificial motor unit  
162 twitch model (Figure 1D). The digital twitch embedded in NeurOne simulates the muscle twitch in  
163 a human muscle and has a latent period, a contraction phase, and a relaxation phase. Our  
164 approach to feedback calculation enabled high accuracy in tracking the requested trajectory (see  
165 paragraph below). We implemented the decomposition and rendering of motor unit activity by  
166 utilizing the high-performance graphical processing unit that enabled the display of the motor unit  
167 feedback and spike trains with real-time resolution  $(32 \frac{\text{frames}}{\text{s}})$ . We then evaluated the performance  
168 of our feedback across the different experiments and in comparison, to intact healthy individuals,  
169 which are described below. Metrics across groups are described as mean±standard deviation.

#### 170 *Accuracy of the neural feedback*

171 All three participants with sensory and motor complete SCI were able to follow the requested  
172 trajectory with high levels of accuracy by modulating task-related motor units. The attempted tasks  
173 involved power grasp (hereafter grasp) for all participants and pinch grasp (hereafter pinch,  
174 S1)/index flexion/extension (hereafter index, S2 and S3) depending on the subject. Figure 2A  
175 shows the participants in the experimental environment with the applied HD-sEMG electrode grids.  
176 Across the first three sessions the Pearson correlation coefficient  $r$  (PCC) and the root-mean-  
177 squared error RMSE are calculated for each task and for the ramps of different levels of activations  
178 (LoA) individually for each ramp/feedback pair. The level of activation (hereafter referred simply to  
179 activation) refers to the extent of motor unit activation, i.e., motor unit discharge rate, relative to the  
180 maximal activation observed during the offline recording. Figure 2B shows the whole recording of  
181 the online session with the highest average correlation  $r$  and lowest average error RMSE per  
182 activation for each participant. The neural feedback trajectory calculated by NeurOne is displayed  
183 in blue and the requested trajectory in the red. The neural feedback trajectories of each participant  
184 follow the requested trajectory with some deviation. The average correlation  $r$  ( $r_1=0.909\pm0.028$ ,  
185  $r_2=0.866\pm0.034$ ,  $r_3=0.860\pm0.072$ ;  $p_{1,2}, r=0.248$ ,  $p_{1,3}, r=0.173$ ,  $p_{2,3}, r=0.974$ ) and error RMSE  
186 ( $\text{RMSE}_1=0.231\pm0.031$ ,  $\text{RMSE}_2=0.280\pm0.081$ ,  $\text{RMSE}_3=0.228\pm0.042$ ;  $p_{1,2}, \text{RMSE}=0.243$ ,  $p_{1,3}$ ,  
187  $\text{RMSE}=0.995$ ,  $p_{2,3}, \text{RMSE}=0.208$ ) throughout their best session for participants S1-S3 were similar,  
188 suggesting that NeurOne provides high proportionality using motor unit spiking activity.





189 **Figure 2.** Performance of the participants in the study. A) The three participants in the study during a session. Two electrode  
 190 grids, each having 64 electrodes are placed on the skin of the forearm of the paralyzed hand. After performing a warm-up  
 191 and recording 20 seconds of high-density surface electromyography (HD-sEMG) the online session is performed. B) The  
 192 best online attempted movements throughout all sessions (a total of nine sessions per task spanning over three training  
 193 days) where the participants followed a requested trajectory (red line) consisting of eight ramps by their task-related motor  
 194 unit activity (blue line). The accuracy of the performance is calculated through the Pearson correlation coefficient  $r$  and the  
 195 root-mean-square error  $RMSE$  per activation. C) Correlation and error were calculated individually for each ramp/feedback  
 196 pair throughout the first three training sessions for all participants shown for each task and differed between the activations  
 197 of 20% and 60%. Ramp/feedback pairs that had a correlation below  $r < 0.5$  were discarded as they were marked as not  
 198 followed. The correlation  $r$  and error  $RMSE$  demonstrated largely consistent patterns between different activation levels and  
 199 tasks. However, it is noteworthy that participant S1 was the only participant showing significant differences between lower  
 200 and higher activations in both metrics.

201 We found a difference between the average  $RMSE$  of the lower (20% of maximum) and higher  
 202 (60% of maximum) activations for participants S1 and S2. Specifically, for S1, we observed a  
 203 significant difference ( $p=0.037$ ) in the average  $RMSE$  between lower ( $RMSE_{1,20}=0.208\pm 0.027$ ) and  
 204 higher ( $RMSE_{1,60}=0.254\pm 0.013$ ) activations. Similarly, for S2, a significant contrast in average  
 205  $RMSE$  values was evident ( $RMSE_{2,20}=0.344\pm 0.061$  vs.  $RMSE_{2,60}=0.216\pm 0.032$ ), with a p-value of  
 206 0.017. These results indicate that accuracy in following ramps is more difficult with lower activations  
 207 than with higher activations.

208 Despite these  $RMSE$  variations, there were no significant differences in correlation  $r$  for both S1  
 209 and S2. The correlation values remained consistent for S1 ( $r_{1,20}=0.904\pm 0.037$  and  $r_{1,60}=0.914\pm 0.011$ , with p-value of 0.684) and S2 ( $r_{2,20}=0.853\pm 0.023$  and  $r_{2,60}=0.879\pm 0.037$ , with p-  
 210 value of 0.335). In the case of participant S3, we found no significant difference between activation  
 211

212 levels for both correlation  $r$  ( $r_{3, 20}=0.824\pm0.071$  and  $r_{3, 60}=0.897\pm0.052$ ) and error  $RMSE$  ( $RMSE_{3, 20}=0.214\pm0.027$  and  $RMSE_{3, 60}=0.338\pm0.009$ ), with p-values of 0.203 and 0.257, respectively.

214 Figure 2C illustrates the overall performance across sessions. All participants displayed a robust  
215 linear relationship between task performance and activation levels, with an average correlation  
216 coefficient exceeding  $r>0.785$ . The correlation was significantly higher at higher activation levels  
217 ( $r_{20}=0.769\pm0.056$ ,  $r_{60}=0.806\pm0.075$ ,  $p=0.024$ ). Notably, participant S1 exhibited a strong linear  
218 relation in both activation levels and tasks ( $r_{1, 20, pinch}=0.853\pm0.051$ ,  $r_{1, 60, pinch}=0.867\pm0.051$ ,  $r_{1, 60, grasp}=0.867\pm0.090$ ), except for the grasp task at 20% maximum activation ( $r_{1, 20, grasp}=0.783\pm0.077$ ), which was significantly lower (p-values in respect to grasp at 20% activation:  $p_{grasp, 60}=1.7e-4$ ,  $p_{pinch, 20}=1.1e-3$ ,  $p_{pinch, 60}=4.7e-5$ ). In contrast, participants S2 ( $r_{2, 20, grasp}=0.696\pm0.158$ ,  $r_{2, 20, index}=0.684\pm0.106$ ,  $r_{2, 60, grasp}=0.724\pm0.146$ ,  $r_{2, 60, index}=0.681\pm0.140$ ) and S3 ( $r_{3, 20, grasp}=0.802\pm0.097$ ,  $r_{3, 20, index}=0.795\pm0.079$ ,  $r_{3, 60, grasp}=0.851\pm0.091$ ,  $r_{3, 60, index}=0.847\pm0.063$ ) did not exhibit significant differences in their correlations between the two different activations and tasks.

225 Regarding error, lower activation levels had generally higher error values, while higher activation  
226 levels had lower error values ( $RMSE_{20}=0.369\pm0.059$ ,  $RMSE_{60}=0.304\pm0.047$ ,  $p=5.3e-7$ ). Notably,  
227 participant S3 demonstrated the lowest error for lower activation levels ( $RMSE_{3, 20}=0.288\pm0.076$ )  
228 and a similar error to participant S1 for higher activation levels ( $RMSE_{1, 60}=0.269\pm0.069$ ;  $RMSE_{3, 60}=0.274\pm0.055$ ). Participant S2 showed similar error values to participant S1 for lower activation levels ( $RMSE_{1, 20}=0.415\pm0.172$ ;  $RMSE_{2, 20}=0.406\pm0.074$ ). However, participant S2 exhibited the highest error for the highest activation levels ( $RMSE_{2, 60}=0.365\pm0.094$ ).

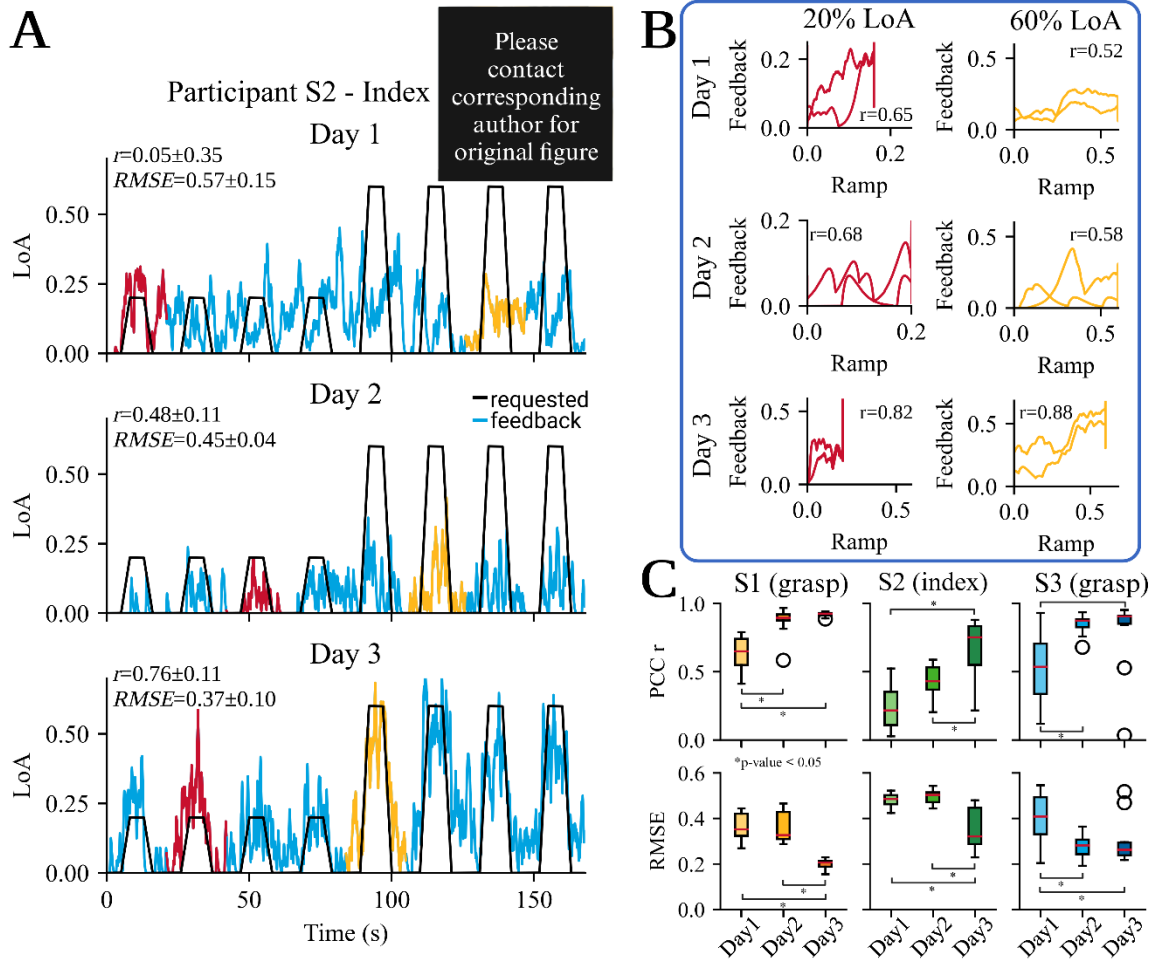
232 Participants S2 and S3 consistently maintained errors in following the requested trajectory, with no  
233 significant differences between higher and lower activations and tasks. However, participant S1,  
234 showed a significant difference between lower and higher activations and tasks ( $p_{grasp60}=0.004$ ,  $p_{grasp20, pinch20}=0.927$ ,  $p_{grasp20, pinch60}=5.42e-6$ ,  $p_{grasp60, pinch20}=0.018$ ,  $p_{grasp60, pinch60}=0.455$ ,  $p_{pinch20, pinch60}=2.92e-5$ ). Moreover, this participant had the lowest overall error for the pinch task at 60% maximum activation ( $RMSE_{1, 60, pinch}=0.246\pm0.034$ ) but also the highest overall error for the grasp task at lower activation levels ( $RMSE_{1, 20, grasp}=0.426\pm0.159$ ) indicating that the lower activations were more difficult to follow for this participant.

240 Additionally, when examining the interquartile range  $IQR$  across all tasks and activations for  
241 correlation, participant S1 demonstrated the lowest  $IQR$  ( $IQR_{1, r}=0.082\pm0.009$ ), indicating a high  
242 level of consistency. Participant S3 followed with a slightly higher  $IQR$  ( $IQR_{3, r}=0.112\pm0.031$ ). In  
243 contrast, participant S2 exhibited a considerably larger range than the other two participants in  
244 correlation ( $IQR_{2, r}=0.223\pm0.068$ ). As for the calculated error  $RMSE$  between the ramp and  
245 feedback, participant S1 had the highest average range across all tasks and activations ( $IQR_{1, RMSE}=0.166\pm0.110$ ). However, this was mainly influenced by the higher ranges for error  $RMSE$  at lower activations ( $IQR_{1, RMSE, 20}=0.245$ ;  $IQR_{1, RMSE, 60}=0.078$ ) emphasising the significant differences between lower and higher activations for participant S1. On the other hand, participant S3 displayed the lowest range across all metrics, tasks, and activations ( $IQR_{3, RMSE}=0.088$ ;  $IQR_{3, r}=0.112$ ). Interestingly, for participant S3, the range for lower activations was smaller compared to higher activations ( $IQR_{3, RMSE, 20}=0.101$ ,  $IQR_{3, RMSE, 60}=0.081$ ,  $IQR_{3, r, 20}=0.135$ ,  $IQR_{3, r, 60}=0.089$ ).

252 These findings illuminate the consistency and variability in participants' performance across tasks  
253 and activation levels, offering valuable insights into individual dissimilarities and patterns of  
254 response. Moreover, we observed a consistent and robust training effect for all subjects. Within  
255 just a few days of using NeurOne, the participants exhibited remarkable improvement, accurately  
256 tracking a prescribed trajectory, as described below.

### 257 *Improvement of neural feedback*

258 Figure 3 illustrates the progress made by the participants during the three training sessions across  
259 three consecutive days that spanned over 2 weeks for participants S2 and S3. For participant 1 the  
260 first two training sessions spanned over 1 week while the last session had to be conducted two  
261 months later. Figure 3A displays the best (highest average correlation across all ramp/feedback  
262 pairs) online session for participant S2 for the index finger on each training day. On the first day,



263 **Figure 3.** The effectiveness of the proposed neural feedback system in improving the accuracy of tracking a requested  
 264 trajectory with a cursor. NeurOne was tested on three participants (S1, S2, and S3) over three training days spanning  
 265 between seven days (S2) up to 2 months (S1). A) shows the improvement in proportional control of motor unit activity over  
 266 time for participant S2. On the first day of training, no proportional control was observed, as feedback was activated even  
 267 when not requested. However, by the second day, the participant was able to activate motor unit activity only when it was  
 268 requested. On the third day, the participant was able to modulate the feedback with high proportionality and low error. B)  
 269 presents the correlation and error values between the best feedback and requested trajectory for each training day for  
 270 participant S2, as calculated from the best correlated feedback/ramp pair in the online recording. The plot demonstrates  
 271 that the correlation improves over the course of the training days. C) Boxplots of the Pearson correlation coefficient  $r$   
 272 and root-mean-square error  $RMSE$  per activation for each participant at 60% of the maximum activation for one task. All  
 273 participants showed a significant increase in the correlation  $r$  ( $\Delta r_1=147.6\%$ ,  $p_1=1.33e-6$ ;  $\Delta r_2=275.6\%$ ,  $p_2=8.16e-4$ ;  
 274  $\Delta r_3=172.9\%$ ,  $p_3=2.44e-3$  for participants S1, S2 and S3 respectively) and a significant decrease in the error from day 1 to  
 275 day 3 ( $\Delta RMSE_1=45.6\%$ ,  $p_1=3.54e-5$ ;  $\Delta RMSE_2=25.6\%$ ,  $p_2=0.011$ ;  $\Delta RMSE_3=37.6\%$ ,  $p_3=2.72e-3$  for participants S1, S2 and  
 276 S3 respectively). Participants S1 and S3 achieved consistent accuracy in following the trajectories, as the range in  
 277 performance at individual ramps decreased ( $\Delta r_1=94.8\%$ ,  $\Delta RMSE_1=64.3\%$ ;  $\Delta r_3=98.6\%$ ,  $\Delta RMSE_3=66.9\%$ ) over the training  
 278 sessions. In contrast, participant S2 showed an increase in the range, but the median values were higher for the correlation  
 279 and lower for the error on day 3 than on the other days.

280 participant S2 had an average correlation  $r_1=0.054\pm 0.351$  and error  $RMSE_1=0.574\pm 0.154$  across  
 281 all feedback/ramp pairs of this session. Moreover, the normalized activation levels from the neural  
 282 feedback remained almost constant throughout the recording. By the second day, the neural  
 283 feedback during the resting phase had become silent, and while the feedback at the requested  
 284 activation of 60% did not reach 60%, the activation level for those ramps was higher than for the  
 285 ramps at 20% of maximum activation. We speculate that the subjects learned to silence the motor  
 286 units with tonic activity (firing when no task was displayed on the monitor) that were observed on  
 287 day 1. The average correlation of  $r_2=0.477\pm 0.108$  and error of  $RMSE_2=0.448\pm 0.041$  was  
 288 significantly improved. On the third day, participant S2 was able to modulate the feedback at the  
 289 requested activation level, and the feedback trajectory tended to overshoot the requested activation



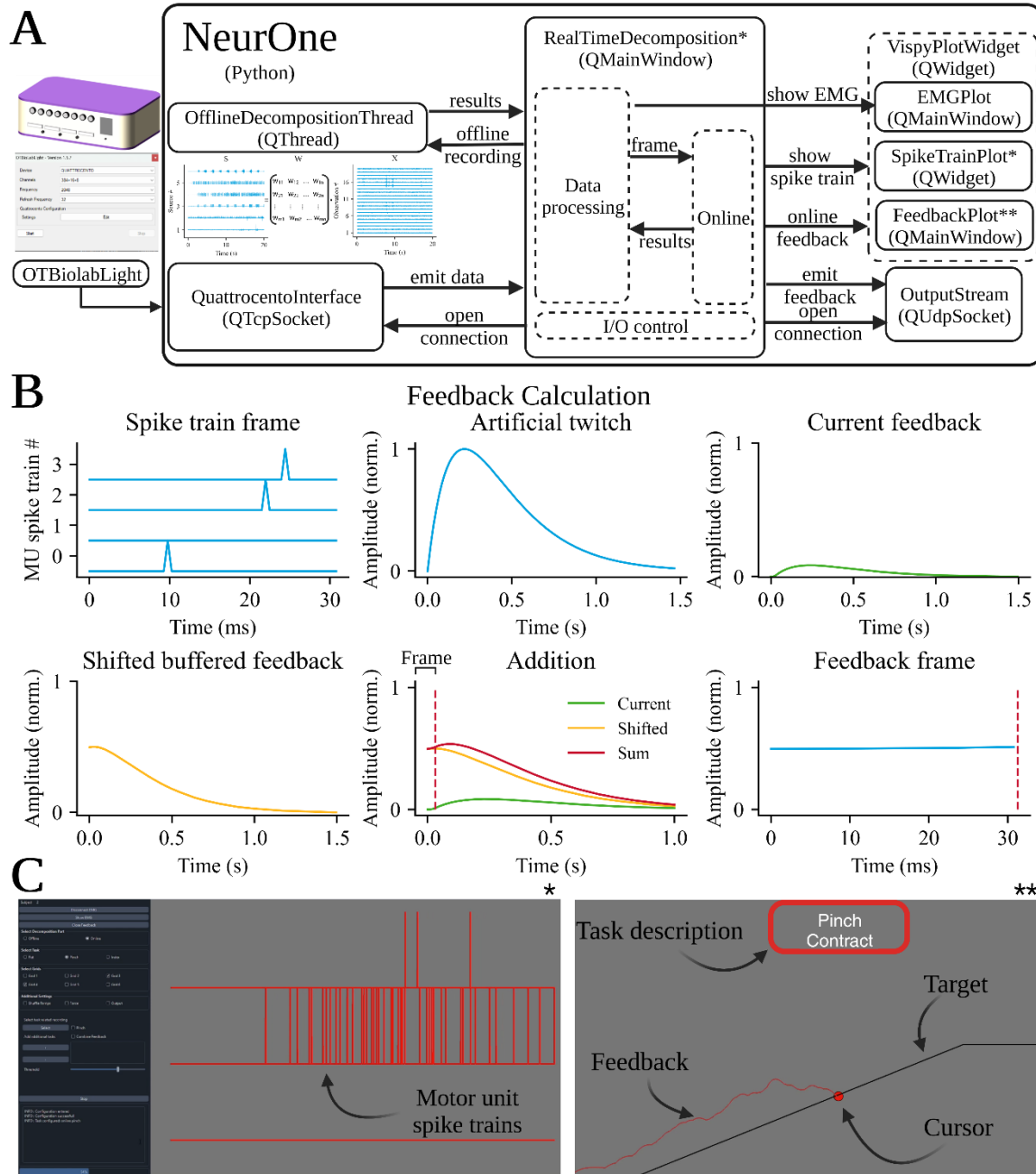
290 Although the neural feedback was still active during the resting phase, the activation was much  
291 lower than during the actual ramps. During the best performance of the index finger task, the  
292 participant had an average correlation of  $r_3=0.759\pm0.109$  and an error of  $RMSE_3=0.372\pm0.104$   
293 across all feedback/ramp pairs of this session. Across the days, participant S2 was able to improve  
294 the proportional control of the cursor by more than 1,400% and reduced the error by 35.2%. Figure  
295 3B shows the requested activation level plotted against the feedback calculated by NeurOne and  
296 displays the differences between the days more clearly. For each day, a ramp/feedback pair with  
297 the highest correlation value was selected for both 20% and 60% activations. The feedback at 20%  
298 of maximum activity is colored red, while the feedback at the requested activation level of 60% is  
299 colored yellow. The activations at 20% on day 1 showed a negative correlation of  $r_{1,20}=-0.20$  for  
300 20% and  $r_{1,60}=-0.14$  for 60% of the maximum activation. By day 2, the correlation for the target  
301 activation level of 20% reached  $r_{2,20}=0.68$  and for 60% the correlation had the value  $r_{2,60}=0.34$ . By  
302 day 3, the correlation for both activation levels reached  $r_{3,20}=0.78$  for 20% and  $r_{3,60}=0.88$  for 60%  
303 of the maximum activation level.

304 Across three days of training, all participants demonstrated a higher correlation and lower error in  
305 at least one task when the activation level was set to 60%. Figure 3C illustrates the performance  
306 of the ramp/feedback pairs, which revealed that on the first day, each participant had a lower  
307 correlation ( $r_{1,day1}=0.626\pm0.141$ ;  $r_{2,day1}=0.246\pm0.215$ ;  $r_{3,day1}=0.525\pm0.284$ ) and higher error  
308 ( $RMSE_{1,day1}=0.362\pm0.063$ ;  $RMSE_{2,day1}=0.479\pm0.042$ ;  $RMSE_{3,day1}=0.402\pm0.105$ ). On the third day,  
309 all participants showed a significant increase in correlation values ( $r_{1,day3}=0.924\pm0.016$ ,  $p=1.33e-$   
310  $6$ ;  $r_{2,day3}=0.678\pm0.208$ ,  $p=8.16e-4$ ;  $r_{3,day3}=0.908\pm0.003$ ,  $p=2.44e-3$ ) and a decrease in error values  
311 ( $RMSE_{1,day3}=0.197\pm0.028$ ,  $p=3.54e-5$ ;  $RMSE_{2,day3}=0.357\pm0.094$ ,  $p=0.011$ ;  $RMSE_{3,}$   
312  $day3=0.251\pm0.032$ ,  $p=2.72e-3$ ). Compared to participant S2, participants S1 and S3 achieved high  
313 correlation values by the second day ( $r_{1,day2}=0.899\pm0.042$ ,  $p_1=9.67e-7$ ;  $r_{3,day2}=0.861\pm0.047$ ,  
314  $p_3=7.82e-4$ ). However, the error was not reduced for participant S1 ( $RMSE_{1,day2}=0.353\pm0.066$ ,  
315  $p=0.938$ ). Overall, there was an increase of 147.6%, 275.6%, and 172.9% in the correlation and a  
316 decrease of 45.6%, 25.6%, and 37.6% in the error for participants S1, S2, and S3, respectively.

317 Furthermore, the interquartile range *IQR* in the results decreased for participants S1 and S3 from  
318 day 1 to day 3. For participant S1, the range in correlation decreased by 94.8% ( $IQR_{1,day1}, r=0.192$   
319 to  $IQR_{1,day3}, r=0.010$ ) and in error by 64.3% ( $IQR_{1,day1}, RMSE=0.098$  to  $IQR_{1,day3}, RMSE=0.035$ ).  
320 Although the range decreased significantly for correlation after one day of training, the error was  
321 only reduced on the third day. For participant S3, the range for correlation and error decreased  
322 after the first day ( $IQR_{3,day1}, r=0.369$  to  $IQR_{3,day2}, r=0.053$ ;  $IQR_{3,day1}, RMSE=0.163$  to  $IQR_{3,day2},$   
323  $RMSE=0.054$ ). From day 1 to day 3, the interquartile range *IQR* in correlation decreased by 98.6%  
324 ( $IQR_{3,day3}, r=0.005$ ) and in error by 66.9% ( $IQR_{3,day3}, RMSE=0.054$ ). However, only participant S2  
325 showed an increase in range and correlation values, but the error values decreased. This was  
326 particularly evident in the error range, which was similar on the first two days ( $IQR_{2,day1}, RMSE=0.040$   
327 to  $IQR_{2,day2}, RMSE=0.044$ ), but increased by 400% on the last training day ( $IQR_{2,day3}, RMSE=0.160$ ).  
328 Regarding the correlation, there was a decrease of 32.8% in the range between the first two days  
329 ( $IQR_{2,day1}, r=0.244$  to  $IQR_{2,day2}, r=0.164$ ), but on the last training day, the correlation range was  
330 significantly increased ( $IQR_{2,day3}, r=0.284$ ).

### 331 *Validation of NeurOne*

332 Figure 4 depicts the software architecture of NeurOne, including the feedback calculation process  
333 for achieving seamless and ultra-fast feedback delivery to the user. The interface to the  
334 amplification device, which records the HD-sEMG signals, enables the streaming of  $32 \frac{\text{frames}}{\text{s}}$  with  
335 a sampling frequency of 2048 Hz (64 data samples per frame) for a total of 408 channels. Offline  
336 decomposition of a 20-second recorded HD-sEMG signal (49,960 data samples per channel) was  
337 completed in  $3:05\pm0:10$  minutes. During online decomposition, the measured time difference  
338 between two frames was  $t_{\Delta\text{frame}}=31.3\pm0.42$  ms, resulting in an average of  $31.9 \frac{\text{frames}}{\text{s}}$ . The measured  
339 time to calculate the feedback was  $t_{\text{calc}}=3.07\pm0.7$  ms. Updating the plot windows for the spike trains  
340 and feedback took  $t_{\text{plot}}=4.33\pm0.7$  ms after the frames were received. Participants in the study did  
341 not report any delay between the attempted task and the displayed feedback.



342 **Figure 4.** Overview of NeurOne's software architecture and the feedback calculation process displayed to the participants.  
 343 A) The software is utilizing the PySide6 Python module and uses a QuattrocentoInterface (based on QTcpSocket) to  
 344 communicate with the amplification device software *OT Biolab Light*. This data is then sent to the main window of NeurOne,  
 345 which handles the graphical user interface (GUI), motor unit spike train plots, and data processing. NeurOne can perform  
 346 either offline or online decomposition of incoming data. The spike trains of all motor units, including those of the main and  
 347 sub-tasks, are displayed in the main window using the SpikeTrainPlot widget, while the calculated feedback is plotted in a  
 348 separate FeedbackPlot window (based on QMainWindow), making it possible to display the monitor specifically for the  
 349 participant in a dual monitor setup. NeurOne can also display the high-density surface electromyographic signals in real-  
 350 time using the EMGPlot window (based on QMainWindow). NeurOne also provides the functionality of streaming the  
 351 calculated feedback through an object of the OutputStream class (based on QUdpSocket), which maps the feedback of the  
 352 selected task on the involved fingers to control a virtual hand or mechatronic systems. B) The feedback calculation that  
 353 enables fast and smooth feedback for controlling the cursor to track the requested trajectory. The identified spike trains of  
 354 the task-related motor units are summed up into a cumulative spike train, which is then convolved with a motor unit twitch  
 355 model. The induced feedback from this frame is then added to the calculated feedback from previous frames. From the  
 356 resulting summed feedback, the first 64 samples, i.e., 31.25 ms (red-dotted line), are taken as the feedback frame. The  
 357 average of the feedback frame is mapped on the cursor. C) Main window of NeurOne's GUI that displays the identified

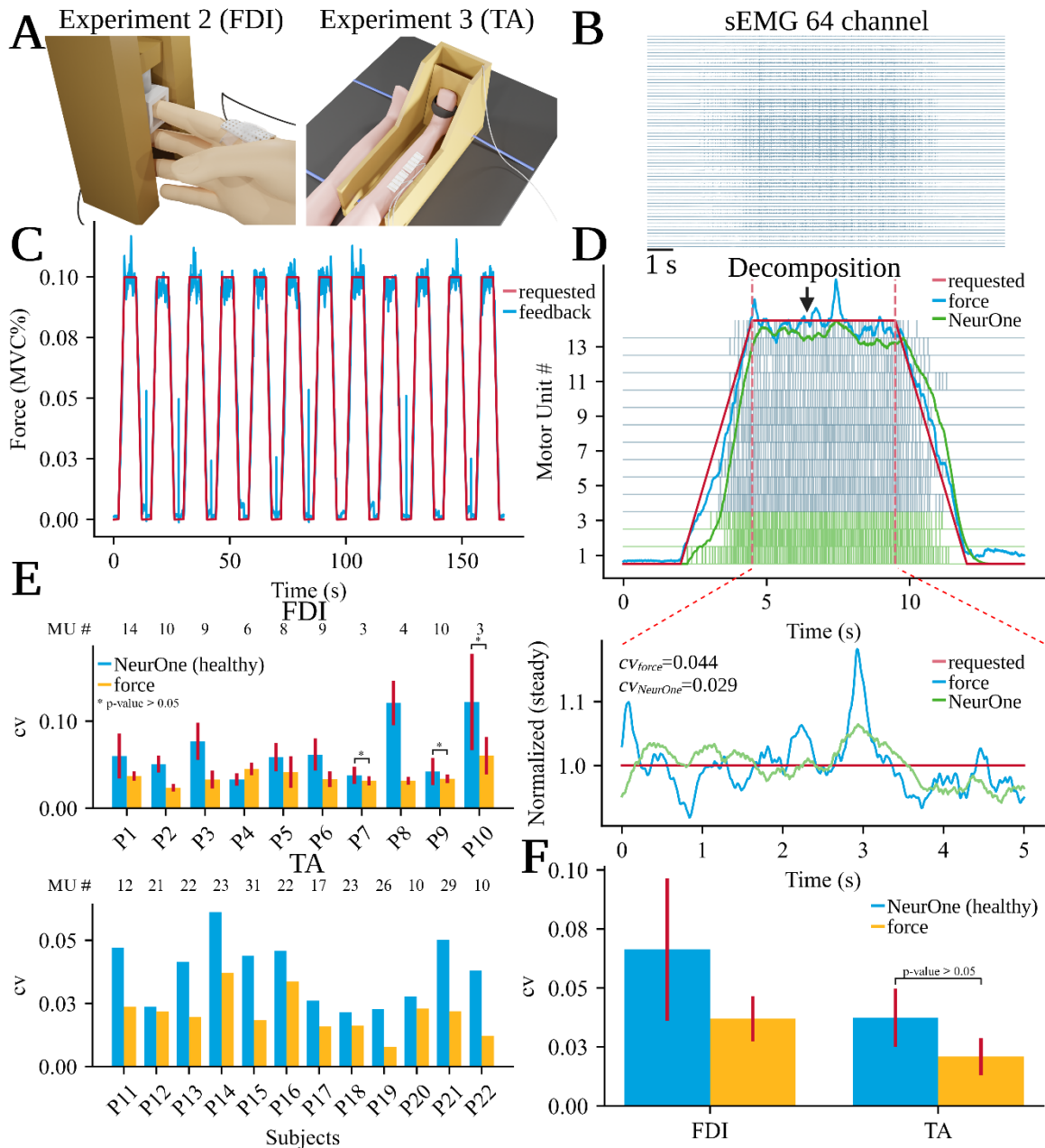
358 motor unit spike trains in real-time (left) and the feedback window that is displayed to the participants of the study (right).  
359 NeurOne's main window allows users to choose tasks, electrode configurations, online and offline parts. In the case of the  
360 online part, users can select one main task from which the feedback is displayed in the feedback window and additional  
361 sub-tasks. The real-time decoded motor unit spike trains are displayed in the main window, with tasks being colored  
362 differently. The feedback window, displayed to the participants in the study, provides task instructions and displays the  
363 cursor (red dot) representing the current feedback frame and its history (red line) while the user is asked to follow the  
364 requested trajectory (black line) by attempting the pinch task.  
365

366 Figure 5 illustrates the validation process of the feedback calculation algorithm integrated in  
367 NeurOne. As previously described, this algorithm uses a motor unit twitch model to smooth the  
368 discharge rates of motor unit firings. To validate this approach, the convolutive feedback method  
369 was applied to decomposed motor unit spike trains of 22 healthy individuals acquired by previously  
370 conducted experiments (10 subjects in the first (10, 25) and 12 subjects in the second experiment  
371 (26, 27)) in an offline analysis. In the second experiment of the study (first experiment with healthy  
372 individuals), the force exerted by the index finger during an isometric contraction was measured  
373 using a mechanical apparatus, while HD-sEMG signals were recorded from the third dorsal  
374 interosseous (FDI) muscle using a 64 channel electrode grid (Figure 5A/B). The second experiment  
375 (second experiment with healthy subjects) involved the measurement of HD-sEMG and force  
376 during isometric ankle dorsiflexion. Two HD-sEMG electrode grids with 64 channels each were  
377 placed on the skin above the musculus tibialis anterior (TA). The force was measured using an  
378 ankle dynamometer.  
379

380 In both experiments, the healthy individuals were instructed to follow a predetermined force  
381 trajectory. For the experiment with the FDI, the requested force trajectory was represented by  
382 twelve ramps with a target activation level of 10% of their maximum voluntary contraction (MVC),  
383 presented in Figure 5C. The MVC was determined prior to the study and one isometric ramp  
384 contraction in the requested trajectory had a duration of 14 seconds. The second experiment with  
385 the ankle dorsiflexion had a target force of 35% MVC with incline and decline of 5%/s and involved  
386 only one ramp.

387 The HD-sEMG signals recorded in both experiments were decomposed into motor unit spike trains,  
388 and the three most active motor units were selected for the validation process. NeurOne's feedback  
389 was derived from analyzing the cumulative spike train of a specific subset of identified motor units,  
390 which was then compared with the recorded force signal (Figure 5D). To simulate the number of  
391 identified motor units in real-time experiments involving SCI, we carefully selected a subpool of  
392 motor units consisting of the three motor units with the highest number of firings during the  
393 contraction phase. The coefficient of variation  $cv$  of NeurOne's feedback was evaluated to  
394 determine its similarity to the coefficient of variation  $cv$  of the measured force signal. Therefore, the  
395 steady parts of the reference signal and NeurOne's feedback were extracted and normalized on  
396 the mean of their respective steady part. The coefficient of variation  $cv$  of the force signal in one  
397 ramp of the first experiment (FDI) was found to be  $cv_{force}=0.044$ , while the coefficient of variation  $cv$   
398 of NeurOne's feedback was  $cv_{NeurOne}=0.078$ .  
399

400 Figure 5E presents an overview of the average coefficient of variation values obtained from the  
401 protocol ramps of experiment 2 (FDI) and 3 (TA). While the coefficient of variation value for the  
402 reference signal in experiment 2 (FDI) was generally lower than the coefficient of variation from  
403 NeurOne's feedback calculation, three healthy participants showed almost similar coefficients of  
404 variation values ( $cv_{P7, force}=0.031\pm 0.005$ ,  $cv_{P7, NeurOne}=0.038\pm 0.010$ ,  $p=0.079$ ;  $cv_{P9, force}=0.034\pm 0.005$ ,  
405  $cv_{P9, NeurOne}=0.042\pm 0.016$ ,  $p=0.105$ ;  $cv_{P10, force}=0.060\pm 0.022$ ,  $cv_{P10, NeurOne}=0.122\pm 0.056$ ,  $p=0.072$ ).  
406 Participant P4 exhibited an even lower coefficient of variation value with NeurOne's feedback than  
407 with the recorded reference signal ( $cv_{P4, force}=0.045\pm 0.007$ ,  $cv_{P4, NeurOne}=0.033\pm 0.007$ ,  $p=6.58e-4$ ).  
408 In experiment 3 (TA) all subjects had a slightly higher coefficient of variation for the calculated  
409 motor unit feedback (NeurOne). Three subjects (P12, P18 and P20), however, showed an almost  
410 similar coefficient of variation  $cv$  to force ( $cv_{P12, force}=0.022$ ,  $cv_{P12, NeurOne}=0.024$ ;  $cv_{P18, force}=0.016$ ,  
411  $cv_{P18, NeurOne}=0.022$ ;  $cv_{P20, force}=0.023$ ,  $cv_{P20, NeurOne}=0.028$ ). However, some subjects (P11, P13-15,  
412 P19, P21-22) had a much higher coefficient of variation  $cv$  for the motor unit feedback of NeurOne  
413 compared to the measured force ( $cv_{P11, force}=0.024$ ,  $cv_{P11, NeurOne}=0.047$ ;  $cv_{P13, force}=0.020$ ,  $cv_{P13,$   
414  $NeurOne}=0.041$ ;  $cv_{P14, force}=0.037$ ,  $cv_{P14, NeurOne}=0.061$ ,  $cv_{P15, force}=0.018$ ,  $cv_{P15, NeurOne}=0.044$ ;  $cv_{P19,$



415 **Figure 5.** Procedure used to validate the feedback calculation method of NeurOne. A) Two experiments were conducted  
 416 that involved placing high-density surface electromyography (HD-sEMG) electrode grids consisting of 64 channels on the  
 417 first dorsal interosseous (FDI) muscle (left) and the musculus tibialis anterior (TA, rechts) of 23 healthy subjects (10 and 12  
 418 in experiment 2 and 3 respectively). At the same time, the isometric force produced during index finger abduction (FDI) and  
 419 ankle dorsiflexion (TA) was measured through a mechanical apparatus. B) A recorded HD-sEMG signal during a ramp  
 420 contraction of experiment 2 (14 seconds) was analyzed and decomposed into motor unit spike trains. C) The subjects were  
 421 instructed to follow a specific trajectory with their generated force, consisting of twelve ramps with a target activation level  
 422 of 10% of maximum voluntary contraction (MVC). The requested trajectory is displayed with the red line and the force  
 423 feedback measured with the blue line (displayed for experiment 2). D) The cumulative spike train of the three motor units  
 424 (green) from the recorded HD-sEMG signal during a ramp contraction of the index finger abduction task were used in the  
 425 feedback calculation approach of NeurOne. Additionally, the requested trajectory (red), the force signal (blue), and the  
 426 feedback calculated by NeurOne (green) are displayed. Four seconds of the plateau part of the ramp (between the vertical  
 427 dotted red lines) were extracted for each signal and experiment and normalized on its mean. Furthermore, the coefficient  
 428 of variation  $cv$  was calculated for the presented ramp plateau. E) The mean and standard deviation of the coefficient of  
 429 variation  $cv$  were calculated for each participant of experiment 2 (FDI, P1-10) and 3 (TA, P11-22) across all ramps. The  
 430 coefficient of variation  $cv$  was displayed for the output of NeurOne's feedback calculation method (blue bars) and the  
 431 recorded force signals (yellow bars) for the healthy subjects. F) Average coefficient of correlation  $cv$  across all participants  
 432 for experiment 2 and 3.



433  $force=0.008$ ,  $CV_{P19, NeurOne}=0.023$ ;  $CV_{P21, force}=0.022$ ,  $CV_{P21, NeurOne}=0.050$ ;  $CV_{P22, force}=0.012$ ,  $CV_{P22,$   
434  $NeurOne}=0.038$ ). Across all healthy subjects during the index finger abduction task, the coefficient of  
435 variation value was  $CV_{FDI, NeurOne}=0.066\pm 0.030$  for the feedback calculation method implemented in  
436 NeurOne. In comparison, the coefficient of variation  $cv$  for force ( $CV_{FDI, Force}=0.037\pm 0.005$ ) was  
437 significantly lower ( $\Delta cv=44\%$ ,  $p=3.51e-3$ ) and exhibited greater consistency with a narrower range  
438 across subjects. This contrasted with the coefficient of variation  $cv$  observed during ankle  
439 dorsiflexion, which was generally lower than during the index finger abduction task. Noteworthy,  
440 when utilizing NeurOne, the coefficient of variation  $cv$  ( $CV_{TA, NeurOne}=0.038\pm 0.012$ ) achieved a similar  
441 value with no significant differences compared to the force during experiment 2 ( $p=0.10$ ) and  
442 experiment 3 ( $CV_{TA, Force}=0.021\pm 0.008$ ,  $p=0.120$ ). These findings suggest the effectiveness of  
443 NeurOne in providing comparable results to force measurements in both experiments.

444 These small discrepancies between the measured force and the rendered force by NeurOne are  
445 related to numerous factors which include a small number of motor units that were used for the  
446 analysis, offline experiments, and other nonlinear characteristics of motor neuron to muscle force  
447 generation. However, the differences in actual force and digitally rendered force by NeurOne were  
448 very small and negligible (Figure 5 D-F).

## 449 Discussion

450 In this study, we introduce NeurOne, a non-invasive and intuitive software that provides users with  
451 immediate neural feedback on the spared motor unit activity, which enabled three SCI individuals  
452 to train and control the spared neural activity after many years of motor complete paralysis. We  
453 presented the framework behind NeurOne which consists of two main parts. We then evaluated  
454 NeurOne on longitudinal experiments and proved that this framework enables SCI individuals to  
455 control a cursor on a screen in a similar way as intact healthy individuals modulate the isometric  
456 force output.

457 The first part of the framework is the offline decomposition that tries to find suitable filters that  
458 extract the source signals, i.e., the motor unit firings convolved with their motor unit action  
459 potentials. The offline decomposition method, which was adapted for NeurOne, a convolutive blind  
460 source separation algorithm, is extensively tested and validated against iEMG by different  
461 researchers (4, 15, 19). The decomposition method is performed fully automatically and requires  
462 only 3 minutes and 5 seconds ( $3:05\pm 0:10$ ) to complete. This makes it considerably faster than  
463 comparable solutions (15).

464 The online decomposition with the intuitive motor unit interface for the paralyzed is the second and  
465 novel part of NeurOne. It applies the found filters from the offline decomposition, i.e., the separation  
466 matrix  $W$ , the motor unit action potentials and the maximum value of the calculated feedback of the  
467 cumulative offline spike train on the streamed HD-sEMG frame. After identifying the motor unit  
468 firings, the task-related cumulative spike train is used to calculate a smooth and super-fast  
469 feedback by convolving it with a motor unit twitch model.

470 Our study demonstrated that NeurOne provides highly effective feedback, enabling participants  
471 with paralyzed hands to accurately follow a requested trajectory with strong proportionality  
472 (correlations of  $r=0.91/0.87/0.86$ ) and minimal error ( $RMSE=0.23/0.28/0.23$  for participants S1/2/3)  
473 across an entire online recording consisting of eight ramps during attempted hand movements.  
474 Note that during these movements the subjects show no movements of the hands (see Ting et al.  
475 and Oliveira et al. for more details on this finding (21, 22)). Furthermore, our results revealed that  
476 NeurOne was capable of motivating and engaging participants to track the requested trajectory  
477 more accurately over the course of multiple training days. For example, participant S2 showed a  
478 substantial improvement in proportionality ( $r=0.05$  to  $r=0.76$ ) and a reduction in error ( $RMSE=0.57$   
479 to  $RMSE=0.37$ ) for the index task over three training days. It should be noted that the reported  
480 correlation and error values are averaged across all eight consecutive ramps in an online recording,  
481 and therefore do not imply that participants were unable to follow any ramp in the first online  
482 sessions. Variability in correlation and error exhibited greater variation during the initial training  
483 sessions. This suggests that as participants became more familiar with the system, their ability to  
484 consistently and accurately track trajectories improved. This training phenomenon highlights the



485 promising utility of NeurOne, which has a direct connection to spinal motor neurons, in the field of  
486 neural rehabilitation for people with paralysis.

487 Consistency in control signals is crucial for the effective use of NeurOne, particularly in applications  
488 involving mechatronic systems such as exoskeletons or prostheses. Individuals with  
489 neuromuscular conditions or paralyzed limbs need a control system that feels natural, and NeurOne  
490 can provide smooth and fast feedback that can be modulated proportionally to different activation  
491 levels within the same time window. The participants achieved an almost similar (no significant  
492 differences for participants S2 and S3, participant S1 has a significant difference for the grasp task  
493 at the lower activation) correlation for both activations across tasks (above  $r > 0.79$  in average)  
494 indicating a strong proportionality between the voluntary motor unit spiking activity and the  
495 requested trajectory. Especially in applications where high durability is crucial, a strong  
496 proportionality between voluntary motor unit spiking activity and target level, along with low error,  
497 becomes vital. This is because maintaining a constantly high activation level would lead to  
498 exhaustion and muscle soreness.

499 However, there are also limitations to the proposed feedback calculation, particularly regarding the  
500 normalization of feedback. The MVC is typically used for this purpose but cannot be calculated  
501 using force sensors in patients with SCI who are not able to produce force with their hands. To  
502 address this, we engaged participants as much as possible during the offline phase through  
503 dynamic contractions and used the maximum value of the calculated offline feedback as the MVC  
504 for normalization. However, there are differences between the online and offline spike detection  
505 methods used in our study, which we plan to address in future studies by using consistent detection  
506 methods.

507 The speed of the feedback calculation and presentation emphasizes the importance of timely  
508 feedback for individuals with SCI, as they do not have visible feedback of their muscle contractions.  
509 Moving average filters are often employed to smooth the discharge rate of motor units for offline  
510 and real-time presentation (15, 22). However, using such filters involves buffering the data, leading  
511 to delays in feedback presentation. In related works, this delay goes up to 500 ms due to the need  
512 to wait for four frames of data at a streaming frequency of 8 Hz (15). Additionally, the low streaming  
513 frequency results in a delayed feedback presentation, with the plot being updated only eight times  
514 per second.

515 NeurOne addresses these limitations by offering a high streaming frequency of 32 Hz, which is  
516 significantly higher than any previous real-time decomposition approaches (15–17, 19), and  
517 introduces significant latencies to the user. The proposed feedback calculation method using a  
518 motor unit twitch model does not require waiting for a specific amount of time, thereby eliminating  
519 the delay in feedback presentation (15).

520 To validate NeurOne's feedback method based on the digital motor unit twitch model, a comparison  
521 in the variability of the signal, i.e., the coefficient of variation  $cv$  during the plateau phase of isometric  
522 ramp contractions in healthy subjects was conducted. In general, the coefficient of variation  $cv$   
523 of the force signals was lower than for smoothed motor unit spiking activity. One reason for the higher  
524 variability observed in the participants is that force feedback was used as a reference to track the  
525 ramp trajectory on a screen, which allowed participants to gauge the steadiness of the force signal.  
526 Moreover, the number of motor units used was limited to the three most active motor units imitating  
527 the number of motor units that were found in individuals with SCI. Together with a high variability  
528 in the number of motor units identified per subject in the decomposition process, this is a limiting  
529 factor in a fair comparison with force measurement as in force generation are up to hundreds of  
530 motor units involved. Another factor that may contribute to higher variability in NeurOne's feedback  
531 is the challenge of reliably identifying small motor units that are generally better in precise and  
532 smooth movements compared to bigger motor units. However, the small motor units are often  
533 suppressed by bigger motor units because of their bigger motor unit action potentials making it  
534 difficult for current decomposition methods to decompose the small motor units (4, 5, 8). Despite  
535 these differences, the variability of NeurOne and the measured torque level was negligible, which  
536 confirms the high robustness of the method for digitalizing motor units in SCI.

537 Nevertheless, a few subjects displayed a similar coefficient of variation  $cv$ , with one subject (P4)  
538 showing even lower variability. This finding is remarkable, given that the human muscle twitch is  
539 optimized for smooth control, resulting in low variability in measured force. This suggests that  
540 NeurOne's feedback is also able to provide real-time smoothness and can be applied to control  
541 assistive devices.

542 An alternative and frequently employed method to control assistive devices, as opposed to the  
543 motor unit twitch model, is the integration of a musculoskeletal model. However, it's important to  
544 note a difference in the torque output bandwidth between musculoskeletal models and actuators of  
545 mechatronic systems. Actuators exhibit a broader torque bandwidth when compared to  
546 musculoskeletal models. Therefore, through the normalization of NeurOne's output, we can  
547 efficiently utilize the complete motor bandwidth, leading to improved performance.

## 548 **Conclusion**

549 In this study, we demonstrated the efficacy of NeurOne, a noninvasive and intuitive software that  
550 provides immediate neural feedback on the spared motor unit activity of individuals with SCI.  
551 Developed with the specific goal of improving the lives of individuals who have paralyzed hands,  
552 NeurOne can help them gain greater control over assistive devices and facilitate communication.  
553 By providing real-time, high-speed, and smooth neural feedback, NeurOne enables individuals with  
554 long-term complete motor paralysis to gain real-time control of their motor unit activity and  
555 accurately track a requested trajectory with a cursor. Our findings suggest that the accuracy of  
556 tracking can be improved through training, indicating the potential for NeurOne to enhance the  
557 rehabilitation process. In addition, we performed offline analysis to validate NeurOne's feedback by  
558 applying it to motor unit spike trains that were decomposed with a high level of accuracy during  
559 isometric index finger abduction and ankle dorsiflexion tasks in healthy participants. We observed  
560 that NeurOne's feedback achieved a level of variability during the plateau phase of the ramps that  
561 was partially similar to the generated force. The smoothness and accuracy of the smoothed motor  
562 unit discharge rate through NeurOne support the possibility of using this software for assistive  
563 device control such as exoskeletons. Overall, our results highlight the promising potential of  
564 NeurOne to revolutionize the way individuals with paralysis interact with the world around them and  
565 improve their quality of life.

## 566 **Materials and Methods**

567 This study involved the recruitment of three participants diagnosed with chronic motor complete  
568 SCI for experiment 1 (SCI subjects). The study employed the following criteria to select participants:  
569 (1) injury level ranging from C4-C6, (2) age between 18 and 60 years old, and (3) absence of  
570 voluntary movement of one hand or both hands. Participant S3 exhibited voluntary hand movement  
571 in their left hand. An overview of the paralyzed participants is shown in Table 1.

572 **Table 1.** Characteristics of recruited participants in the study

Subject	Age range (years)	Gender	Injury level	AIS	Sensory level*	Wrist movement	Time since injury (years)
S1	31-35	M	C5	B	C5	yes	9.1
S2	36-40	F	C5	A	C5	yes	24.2
S3	56-60	M	C5	A	T3	no	6.9

573 \* The sensory level corresponds to lowest level with normal sensory function.

574

575 22 healthy subjects were recruited for experiment 2 (*index finger abduction*, 10 subjects) and  
576 experiment 3 (*ankle dorsiflexion*, 12 subjects). All procedures were conducted in accordance with  
577 the Declaration of Helsinki and were approved by the Ethical Committees of Friedrich-Alexander-  
578 Universität (approval no. 22-138-Bm, experiment 1), Imperial College London (approval no.  
579 18IC4685, experiment 2) and University Rome 'Foro Italico' (approval no. 44 680, experiment 3).

580 Prior to participation, all subjects provided written informed consent. Some data from this study  
581 have been previously published (10, 25–27).

#### 582 *Experiment 1 (spinal cord injury)*

583 The first experiment comprised multiple sessions for each participant, with S2 and S3 undergoing  
584 training on four separate days and S1 on three days. The last session for S1 occurred two months  
585 after the previous sessions, which were conducted within a two-week timeframe. During the  
586 sessions, we trained participants to enhance their neural control over two distinct tasks, utilizing an  
587 online decomposition approach to analyze a HD-sEMG signal obtained from the placement of 128  
588 HD-sEMG electrodes on the forearm's skin. The training tasks consisted of a power grasp, which  
589 involved the flexion and extension of the whole hand, and a pinch grasp that required the  
590 involvement of the thumb and index finger (for S1) or single-digit movement of the index finger (for  
591 S2 and S3). Participant 3 only attempted the training with the power grasp task in the first session.

592 Prior to commencing the training, participants underwent a one-minute warm-up in which they  
593 followed a virtual hand attempting the task in a relatively slow (0.5 Hz), sinusoidal pattern displayed  
594 on a monitor. Subsequently, we recorded a 20-second signal during which participants were asked  
595 to attempt the requested task dynamically, i.e., flexion and extension in repetition. The task was  
596 attempted dynamically during the recording because the decomposition had a higher accuracy at  
597 finding motor units compared to isometric tasks. The recorded signal was then decomposed offline  
598 to determine the unique motor unit action potentials and separation matrix  $W$  for the online phase.  
599 If decomposition was not finding filters or the filters were insufficient, decomposition results of the  
600 same tasks in previous sessions were selected.

601 Once offline decomposition was completed, we initiated the online phase, which comprised three  
602 sets, with each set including eight trajectories, and a one-minute break between sets. The  
603 trajectories consisted of ramps with increasing (three seconds) and decreasing (three seconds)  
604 flanks, as well as a plateau (five seconds). A ten-second resting phase separated each ramp. The  
605 first four ramps had an activation level of 20%, while the subsequent four ramps had an activation  
606 level of 60%. This difference in activation levels was intended to determine whether participants  
607 with paralyzed hands can voluntarily modulate their motor unit activity to match two significantly  
608 different target levels. Moreover, by having the ramps reach two different activation levels, we were  
609 able to test the proportionality at different modulating rates. The relatively long sloping parts with a  
610 duration of three seconds ensured a large period of proportional tracking. The total duration of one  
611 set was 2:48 minutes.

612 In each session for each task, the protocol included a warm-up period followed by the offline  
613 decomposition phase and the online training segment. Between the completion of one task and the  
614 commencement of another, a larger break of three minutes was provided. Altogether, the training  
615 per day took approximately 40-45 minutes.

#### 616 *Experiment 2 (index finger abduction)*

617 The full details of this experiment have been described previously (10, 25). We also provided a  
618 brief explanation of the methods here. A chair, table, and computer monitor constituted the  
619 experimental setup, where participants (nine men and one woman) assumed a comfortable seated  
620 position. Their dominant hand was supported by a custom apparatus, with the forearm immobilized  
621 and positioned between pronation and supination. The index finger and thumb were aligned along  
622 the forearm's longitudinal axis, and a monitor situated 60 cm away displayed the applied force.  
623 Force measurements of the index finger and thumb were captured using a three-axis force  
624 transducer (Nano25, ATI Industrial Automation), which underwent digitization at 2048 Hz (USB-  
625 6225, National Instruments) and underwent low-pass filtering at a cutoff frequency of 15 Hz. HD-  
626 sEMG signals were obtained from the first dorsal interosseous (FDI) and thenar muscles (flexor  
627 pollicis brevis and abductor pollicis brevis) using flexible electrode grids featuring 13x5 electrodes  
628 with a 4 mm interelectrode spacing and amplified with a multichannel amplifier (Quattrocento, OT  
629 Bioelettronica; 16-bit A/D converter, bandwidth 10-500 Hz). Next, the HD-sEMG signals were

630 processed using a well-established BSS algorithm to decompose them into individual motor unit  
631 spike trains (5, 6).

632 Participants engaged in force-matching tasks, involving simultaneous abduction of the index finger  
633 and flexion of the thumb, for a duration of 60 seconds. Visual feedback was provided via a moving  
634 dot cursor on the monitor, with the x-axis representing thumb force and the y-axis representing  
635 index finger force. Participants were instructed to maintain the force signal within 10% of the target  
636 for each applied force.

637 Prior to the tasks, MVC recordings were performed, and two 60-second trials were conducted with  
638 30 seconds of rest between them. The experimental design aimed to explore the extent of common  
639 synaptic inputs among sets of motor neurons, requiring participants to exert forces in the same  
640 sagittal plane for both muscle sets, necessitating approximately 10 minutes of practice.

#### 641 *Experiment 3 (ankle dorsiflexion)*

642 The full details for this experiment have been described previously (26, 27). We also provided a  
643 brief explanation of the methods here. The experimental setup consisted of a custom-made ankle  
644 ergometer (OT Bioelettronica, Turin, Italy) fixed to an examination table using adjustable straps.  
645 Twelve recreationally active young men participated in the study, with their dominant leg secured  
646 to the ergometer using straps (approximately 3 cm width) at the foot, ankle, and knee. Force signals  
647 were recorded using a force transducer (CCt Transducer s.a., Turin, Italy), amplified (200 x), and  
648 sampled at 2048 Hz using an external A/D converter (Quattrocento, OT Bioelettronica, Turin, Italy).  
649 Visual feedback was provided via a custom LabVIEW software (LabVIEW 8.0; National  
650 Instruments, Austin, TX, USA) displayed on a monitor positioned 1 m away from the participants.  
651 HD-sEMG signals were recorded from the TA muscle using two semi-disposable adhesive grids,  
652 each with 64 electrodes (13x5 electrodes with an IED of 8 mm, OT Bioelettronica). The signals  
653 were sampled at 2048 Hz, bandpass filtered (10-500 Hz), and digitally converted using a 16-bit A/D  
654 converter. The HD-sEMG signals were then similar to experiment 2 processed using a well-  
655 established BSS algorithm to decompose them into individual motor unit spike trains (5, 6).

656 Participants underwent a standardized warm-up, consisting of eight isometric contractions of the  
657 dorsiflexors at varying intensities ( $4 \times 50\%$ ,  $3 \times 70\%$ ,  $1 \times 90\%$ ), separated by 15–30 seconds. After  
658 the warm-up, they performed three or four MVCs with 30 seconds of rest in between. The highest  
659 MVC force determined the maximal voluntary force (MVF) used to set target forces (35%, 50%,  
660 and 70% of MVF) for subsequent submaximal contractions. Participants later performed  
661 trapezoidal contractions, gradually increasing to the target force, maintaining it for 10 seconds, and  
662 then linearly decreasing back to the resting force at the same rate. Two trials were conducted for  
663 each target force in randomized order and 3–5-minute rest intervals.

#### 664 *Evaluation of experiment 1 (spinal cord injury)*

665 The analysis of the training sessions was carried out using Python 3.11, where each ramp/feedback  
666 trajectory pair of the online recordings was partitioned and evaluated individually. The trajectories  
667 were then categorized into 20% and 60% activation levels for further analysis. To evaluate the  
668 accuracy of each ramp/feedback trajectory pair, two metrics were used, namely Pearson correlation  
669  $r$  and root-mean-square error  $RMSE$ . Pearson correlation measures the correlation between the  
670 requested (ramp) and actual (feedback) trajectories, indicating the degree of proportionality  
671 between the two. Additionally, the error provides a measure of accuracy by assessing the distance  
672 between the requested and actual trajectories.

673 To enable comparison between participants, the initial three sessions were selected from  
674 participants S2 and S3, resulting in 36 ramp/feedback pairs for each task and activation level. To  
675 demonstrate the overall performance of participants during the online sessions (Figure 2C),  
676 ramp/feedback pairs with a correlation value below 50% were discarded. Boxplots were then used  
677 to plot the ramp/feedback pairs for each task, activation level, and participant, with the box  
678 representing the IQR and the median displayed as a red line. The whiskers extending from the box  
679 represent the minimum and maximum values of the data that fall within 1.5 times the IQR from the  
680 first and third quartile, respectively. The range of the data was described by reporting the IQR, as



681 well as the mean and standard deviation of the ramp/feedback pairs. The mean and standard  
682 deviation were also calculated across all ramp/feedback pairs within the online recording, which  
683 included eight ramp/feedback pairs.

684 To evaluate training improvement, only ramp/feedback pairs with a positive correlation were  
685 considered. Similar to the general performance, the Pearson correlation coefficient  $r$  and the root-  
686 mean-squared error  $RMSE$  were used to describe the accuracy of the tracking. For each training  
687 day, twelve ramp/feedback pairs were evaluated. The best online recordings of participant S2 were  
688 selected based on the highest correlation values across the entire online recording. Mean and  
689 standard deviation were reported for the entire online recording, and the ramp/feedback pairs  
690 selected for the correlation plots (Figure 3B) were based on the highest correlation values within  
691 the online recording.

#### 692 *Evaluation of experiment 2 (index finger abduction) and 3 (ankle dorsiflexion)*

693 The decomposed motor unit pulses and the measured reference signal (i.e., the force) of the  
694 healthy participants were used to validate the feedback calculation approach proposed in our study.  
695 To do this, we calculated the coefficient of variation  $cv$ , which is the ratio of the standard deviation  
696  $\sigma(x)$  to the mean of the reference signal  $x$  during the steady plateau of the trajectory:

$$697 \quad cv = \frac{\sigma(x)}{\mu(x)}.$$

698 Additionally, we calculated the feedback offline, instead of online as in experiment 1, by convolving  
699 the decomposed spike trains of the three most firing motor units with the motor unit twitch model.  
700 Three motor units were selected as this is the average number of motor units identified in our study  
701 in people with SCI. Afterwards, we extracted the steady part and calculated the coefficient of  
702 variation  $cv$ . For each participant, we calculated the mean and standard deviation for feedback and  
703 reference signal (force) across the ramps (twelve ramps per subject for experiment 2 and the best  
704 ramp at 35 % MVC for the subjects in experiment 3). In experiment 2 the ramps that didn't show  
705 three individual motor units spiking during the plateau phase were discarded.

#### 706 *High-density surface electromyography recording*

707 During all sessions of experiment 1, we placed two HD-sEMG electrode grids, each containing 64  
708 electrodes, on the shaved and cleaned skin of the forearm. The electrode grids utilized in our  
709 investigation were square in shape, with an 8x8 configuration of electrodes, and an interelectrode  
710 distance (IED) of 10mm (GR10MM0808, OT Bioelettronica, Turin, Italy). To ensure consistent  
711 electrode placement, we positioned one electrode grid above the extensor digitorum and the  
712 second above the flexor digitorum superficialis, both aligned with the ulna bone. To further enhance  
713 reproducibility, we recorded the exact electrode positions by capturing images. To affix the  
714 electrode grids to the skin, we used bi-adhesive foam layered between the grids and the skin, filled  
715 with conductive paste (SpesMedica, Battipaglia, Italy), and secured them to the forearm using tape.

716 The HD-sEMG signals were recorded using a multichannel amplifier with 16-bit A/D conversion  
717 (Quattrocento, OT Bioelettronica). We used the OT Biolab Light software (OT Bioelettronica) to  
718 record the signals in monopolar mode, with a sampling frequency of 2048 Hz, and filtered by a  
719 bandpass of 10-500 Hz. 408 channels were streamed in real-time using a Transmission Control  
720 Protocol/Internet Protocol (TCP/IP) with a streaming frequency of 32 Hz. However, only the 128  
721 channels holding the HD-sEMG signals were extracted and used from the streamed data.

#### 722 *Online decomposition*

723 The first part of the online decomposition process aiming at the decoding of HD-sEMG signals into  
724 individual firings of motor units in real-time, involved an offline decomposition. The offline  
725 decomposition is necessary to determine the filters that will be applied during the second part of  
726 the process in real-time. Therefore, we conducted a recording of a dynamic task (grasp or  
727 pinch/index finger flexion/extension) and decomposed the recorded HD-sEMG signals.



728 The approach of the decomposition (offline and online) is based on the theoretical model of  
729 measured HD-sEMG signals. The HD-sEMG signal is a convolutive mixture of motor unit spike  
730 trains and action potentials. In matrix form it is described as:

$$731 \quad x(k) = \sum_{l=0}^{L-1} H(l)s(k-l) + n(k),$$

$$732 \quad k = 0, \dots, D_R$$

733 where  $x(k) = [x_1(k), x_2(k), \dots, x_m(k)]^T$  is the vector comprising all recorded observations (HD-sEMG  
734 channels)  $m$  and  $s(k) = [s_1(k), s_2(k), \dots, s_n(k)]^T$  is the vector comprising the spike trains of all motor  
735 units  $n$ . Matrix  $H(l)$  has the size  $m \times n$  for each sample  $l$  and carries the information of the motor  
736 unit action potentials.  $L$  is the duration of the action potentials. Furthermore,  $H(l)$  is assumed to be  
737 constant during the recording of observations. The additive noise vector  $n(k) = [n_1(k), n_2(k), \dots,$   
738  $n_m(k)]^T$  comprises the noise for each observation.  $D_R$  is the duration of the recording of the  
739 observations. By applying BSS techniques to this mixed model, the sources, i.e., the individual  
740 motor units, can be decomposed. For those algorithms, we assume that the identified sources are  
741 not fully correlated and are either sparse or independent (4). The algorithm that we were using for  
742 the offline decomposition of the HD-sEMG was based on the proposed convolutive BSS approach  
743 of Negro et al. (4). To reduce the noise in the observations we applied a Butterworth bandpass filter  
744 (20-500 Hz) to remove noisy frequencies where the observations are not significantly represented  
745 and a 50 Hz notch filter to remove power line interference. Following the filtering, we performed  
746 convolutive sphering as described by Negro et al. (4). The convolutive sphering method involves  
747 extension, centering, and whitening of the HD-sEMG signal. We used an extension factor of  $R=10$   
748 as we were looking for  $n=32$  sources by using  $m=128$  channels and an estimated action potential  
749 length of  $L=40$  samples by following the general equation for the extension factor  $R$  (4):

$$750 \quad R = \frac{n}{m} L.$$

751 The convolutive sphering is followed by applying FastICA, which is a fixed-point iteration algorithm  
752 that maximizes the number of uniquely identified sources, i.e., the mixture of the motor unit spike  
753 trains convolved with its action potential, by using Gram-Schmidt Orthogonalization. Through  
754 FastICA, a separation matrix  $W$  is obtained and by multiplying it with the extended HD-sEMG signal  
755  $\hat{x}(k)$  it results in the source signals  $s(k)$ :

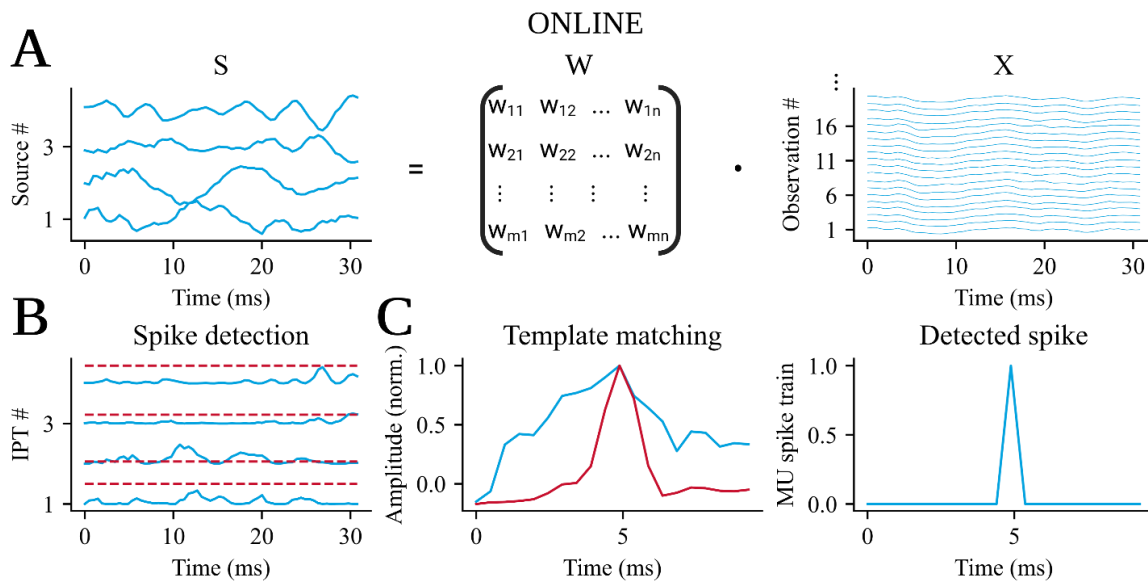
$$756 \quad s(k) = W\hat{x}(k)$$

757 A silhouette score-based K-means driven approach is used to detect spikes from identified sources.  
758 The sources are squared, resulting in innervation pulse trains (IPTs). The peaks of the IPTs are  
759 divided into two classes: high peaks and small peaks. The small peaks, representing noise, are  
760 discarded. High peaks with a silhouette score of 0.9, indicating the distance between spike and  
761 noise, are considered as firing a motor unit.

762 Apart from the optimized separation matrix  $W$  obtained through FastICA, other results from the  
763 offline decomposition are also used in the online part. By calculating the spike triggered average  
764 (STA) for each source, we can find the motor unit action potentials to use in the real-time  
765 decomposition as templates for template matching.

766 To normalize the feedback calculated during the online part, a reference value is required. Without  
767 normalization, an estimation of the activation is not possible. Therefore, feedback using the offline  
768 spike trains is calculated. The feedback is the convolution of the cumulative spike train of all motor  
769 units that are found with an artificial motor unit twitch, which is simulating a muscle twitch during  
770 neural input-based contraction in humans. The real-time detection of spikes from individual motor  
771 units constitutes the second part of the online decomposition, and the pipeline is described in Figure  
772 6. The observations  $x(k)$  in this phase consists of the streamed HD-sEMG frame (128 channels  $\times$   
773 64 samples), which is extended and centered similar to the offline decomposition but not whitened

774 due to high computational costs. The extended observations  $\hat{x}(k)$  are then multiplied with the  
 775 separation matrix  $W$  determined during the respective task in the offline decomposition to obtain  
 776 the identified sources in real-time (Figure 6A). In order to detect spikes in the current frame, the  
 777 sources are subject to thresholding with a threshold value  $T$  set at 10 times the noise level, which  
 778 is calculated in the first frame during rest by taking the average of each source signal in this frame  
 779 (Figure 6B). However, thresholding alone may not be sufficient for reliable spike detection due to  
 780 the lack of filtering of noise through a Butterworth bandpass filter in real-time compared to offline  
 781 decomposition. To enhance the algorithm's reliability, we used template matching (Figure 6C). In  
 782 template matching, spike triggered action potentials of each source were correlated to the motor  
 783 unit action potential extracted during offline decomposition. If the correlation between the template  
 784 and the signal exceeds 0.6, the spike was accepted as valid. Subsequently, the spikes in the current  
 785 frame are convolved with the artificial motor unit twitch used in the offline part. However, since the  
 786 twitch length is significantly longer than the actual frame, the leftover signal is buffered for the next  
 787 frames to prevent an unstable feedback signal. The feedback from the previous frames is then  
 788 shifted and added to the convolutive result in each iteration.



789 **Figure 6.** This figure depicts the online decomposition method that is utilized in our software, NeurOne. The process involves  
 790 three steps. A) First, the source signals are identified in real-time by applying the separation matrix  $W$ , which was discovered  
 791 in the offline stage on the extended and centered high-density surface electromyographic (HD-sEMG) signals of the current  
 792 frame. B) Next, a spike detection technique is applied to the identified sources. This method detects the peak in the  
 793 innervation pulse trains (IPTs), which are the squared source signals of this frame. If the peak of the IPT is greater than 10  
 794 times the noise level, it is designated as a possible spike. C) Finally, template matching is conducted to verify whether the  
 795 possible spike is a motor unit firing or not. To achieve this, a window is implemented around this possible spike in the source  
 796 signal and then correlated with the motor unit action potential that was identified in the offline stage. If the correlation  
 797 coefficient  $r_{\text{threshold}} > 0.60$ , the spike is identified as a motor unit firing.

### 798 Graphical user interface

799 NeurOne is a software that provides a GUI for real-time display of identified motor unit firings and  
 800 neural feedback. Figure 4A shows the architecture of the back-end of NeurOne. NeurOne is written  
 801 in Python 3.10 and utilizes the PySide6 module which provides access to the complete Qt 6.0+  
 802 framework. The RealTimeDecomposition class, which is a child class of QMainWindow, integrates  
 803 the GUI and the back-end, and manages the flow of data within NeurOne for processing and  
 804 plotting.

805 The study, in which NeurOne was used, involved recording and amplifying HD-sEMG signals from  
 806 the participant's forearm using a multichannel amplification system (Quattrocento, OT  
 807 Bioelettronica, Italy). The communication between the recording software (OT Biolab Light) and  
 808 NeurOne was established via TCP/IP network communication using the QuattrocentoInterface  
 809 class. Depending on the selected part (offline or online decomposition), the input frame is either  
 810 directly decomposed in real-time or buffered for offline analysis after recording. The online

811 processed HD-sEMG frame, which is the motor unit spike train, is displayed in the SpikeTrainPlot  
812 widget. Furthermore, the feedback is calculated by the convolution of the motor unit spike trains  
813 with the motor unit twitch model (Figure 4B) and displayed in the FeedbackPlot window. These  
814 visualizations are based on the VispyPlotWidget class, which uses the graphical processing unit  
815 (GPU) to render the data. This is enabled by the VisPy library in Python. Furthermore, the EMGPlot  
816 is a separate window that can be opened and configured to display the streamed HD-sEMG signals  
817 and is based on the VispyPlotWidget too. Additionally, NeurOne uses the OutputStream class to  
818 open a UDP socket to stream the calculated feedback as a control signal to control a virtual hand  
819 or assistive devices. After the offline and online recordings, the results are stored in a NumPy file  
820 (.npy extension) along with a timestamp and subject identifier for subsequent data processing.  
821 NeurOne's GUI is shown in Figure 4C. The user can connect to the HD-sEMG measurement  
822 system, display streamed data in real-time, and start the neural interface to follow requested  
823 trajectories with the feedback cursor. Furthermore, the selection of the offline or the online part is  
824 enabled through radio buttons. The user can configure the HD-sEMG by selecting respective  
825 channel ports that are connected to the electrodes placed on the forearm and repeat the offline  
826 part until the identified filters are reliable and provide great accuracy in the online part. Tasks  
827 available to the user are grasp and pinch as well as index flexion/extension. In the online part, the  
828 user can choose filters for the main task by choosing the respective folder in the operating system's  
829 filesystem. The main task determines which task the subject should attempt to follow the requested  
830 trajectories. Additionally, sub-tasks may be selected, whose motor unit firings are displayed  
831 alongside the main task, but without real-time display of the feedback. The requested trajectory  
832 that is used for the online protocol has four ramps with a low activation of 20% followed by four  
833 high ramps with an activation of 60%. The requested trajectory and the corresponding feedback  
834 trajectory were displayed on the FeedbackPlot window, which was located on a second monitor in  
835 front of the participants.  
836 The evaluation of the computing and plotting time was done on a mobile laptop (XMG NEO 15 E21,  
837 Ryzen 9 5900HX, NVIDIA RTX 3080 mobile, 32 GB Ram), on which 15 motor units were recorded  
838 and visualized during the measurement. The display of spike trains and feedback had a window of  
839 5 seconds and 128 channels of HD-sEMG were decomposed.

#### 840 *Statistical Analysis*

841 In this study, we conducted statistical analyses to investigate significant differences in the  
842 measured results using one-way ANOVA type 2 (for more than two groups) with the `anova_lm`  
843 function from the Python package `Statsmodel` and t-test (for two groups) with the `ttest_ind` function  
844 from the Python package `Scipy`.

845 We employed the significance level  $\alpha=0.05$  to determine whether there are significant differences  
846 between groups. P-values below the significance level indicate the rejection of the null  
847 hypothesis, highlighting observable significant differences. Conversely, p-values above the  
848 significance level indicate no difference in the data. To identify specific group differences after the  
849 one-way ANOVA, we conducted a pairwise Tukey test using the `pairwise_tukeyhsd` function from  
850 the Python package `Statsmodel`. In Experiment 1, we applied the statistical analysis to detect  
851 differences between lower and higher activations and between different tasks. The correlation  
852 coefficient  $r$  and error  $RMSE$  were used individually as dependent variables to assess their  
853 significance. Additionally, the analysis was used to highlight significant improvements over the  
854 training days. In Experiment 2, the statistical analysis aimed to identify significant differences  
855 between the coefficient of correlation  $cv$  (dependent variable) of the feedback calculated using the  
856 method implemented in NeurOne and the recorded force. Moreover, we conducted a statistical  
857 analysis across all participants in Experiments 2 and 3 to investigate significant differences in the  
858 variability of force and motor unit feedback.

859 **Acknowledgments**

860

861 This study was partly funded by d.hip (Digital Health Innovation Platform), a cooperation between  
862 Siemens Healthineers, Medical Valley, University Hospital Erlangen, and Friedrich-Alexander  
863 University Erlangen-Nuremberg, and the German Aerospace Center (DLR) as part of the  
864 MYOREHAB project.

865

866 **Data Availability**

867 All data produced in the present study are available upon reasonable request to the authors. An  
868 executable of NeurOne can be found [here](#)<sup>1</sup>.

<sup>1</sup>Link: <https://github.com/NsquaredLab/NeurOne>

## 869 References

870

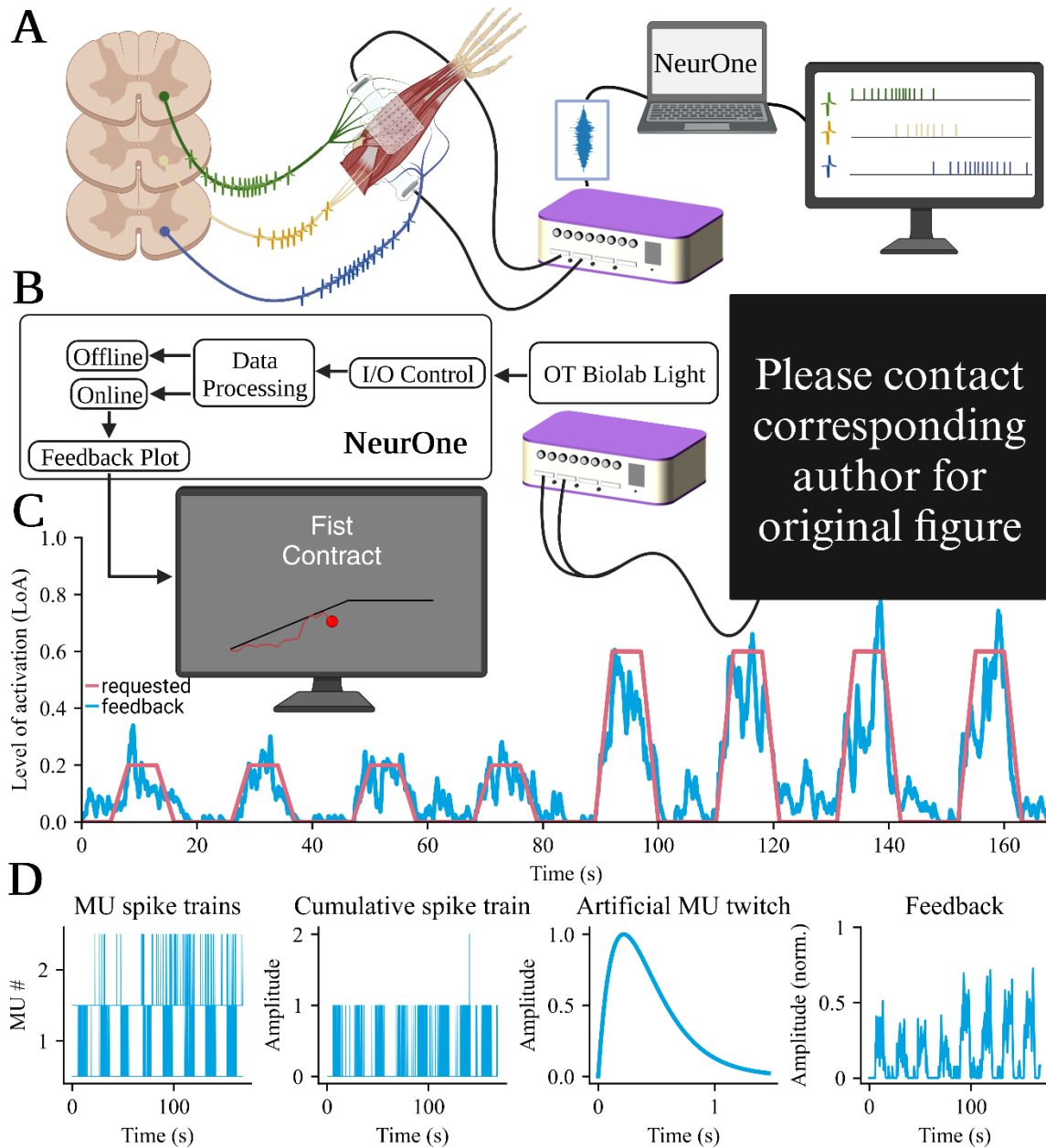
- 871 1. R. Merletti, S. Muceli, Tutorial. Surface EMG detection in space and time: Best practices.  
872 *Journal of Electromyography and Kinesiology* **49**, 102363 (2019).
- 873 2. R. Merletti, G. L. Cerone, Tutorial. Surface EMG detection, conditioning and pre-  
874 processing: Best practices. *Journal of Electromyography and Kinesiology* **54** (2020).
- 875 3. M. Chen, P. Zhou, A Novel Framework Based on FastICA for High Density Surface EMG  
876 Decomposition. *IEEE Transactions on Neural Systems and Rehabilitation Engineering* **24**,  
877 117–127 (2016).
- 878 4. F. Negro, S. Muceli, A. M. Castronovo, A. Holobar, D. Farina, Multi-channel intramuscular  
879 and surface EMG decomposition by convolutive blind source separation. *J Neural Eng* **13**  
880 (2016).
- 881 5. A. Holobar, D. Farina, Blind source identification from the multichannel surface  
882 electromyogram. *Physiol Meas* **35**, R143–R165 (2014).
- 883 6. A. Holobar, D. Zazula, Multichannel Blind Source Separation Using Convolution Kernel  
884 Compensation. *IEEE Transactions on Signal Processing* **55**, 4487–4496 (2007).
- 885 7. A. Holobar, D. Zazula, “Gradient Convolution Kernel Compensation Applied to Surface  
886 Electromyograms” in *Independent Component Analysis and Signal Separation*, (Springer  
887 Berlin Heidelberg, 2007), pp. 617–624.
- 888 8. D. Farina, A. Holobar, Characterization of Human Motor Units From Surface EMG  
889 Decomposition. *Proceedings of the IEEE* **104**, 353–373 (2016).
- 890 9. A. Del Vecchio, *et al.*, Tutorial: Analysis of motor unit discharge characteristics from high-  
891 density surface EMG signals. *Journal of Electromyography and Kinesiology* **53** (2020).
- 892 10. A. Del Vecchio, *et al.*, The Forces Generated by Agonist Muscles during Isometric  
893 Contractions Arise from Motor Unit Synergies. *The Journal of Neuroscience* **43**, 2860–  
894 2873 (2023).
- 895 11. D. S. de Oliveira, *et al.*, Neural decoding from surface high-density EMG signals: influence  
896 of anatomy and synchronization on the number of identified motor units. *J Neural Eng*  
897 **19**, 046029 (2022).
- 898 12. A. Del Vecchio, *et al.*, You are as fast as your motor neurons: speed of recruitment and  
899 maximal discharge of motor neurons determine the maximal rate of force development  
900 in humans. *Journal of Physiology* **597**, 2445–2456 (2019).
- 901 13. V. Glaser, A. Holobar, Motor Unit Identification From High-Density Surface  
902 Electromyograms in Repeated Dynamic Muscle Contractions. *IEEE Transactions on Neural*  
903 *Systems and Rehabilitation Engineering* **27**, 66–75 (2019).
- 904 14. A. L. Cakici, *et al.*, A Generalized Framework for the Study of Spinal Motor Neurons  
905 Controlling the Human Hand During Dynamic Movements in *2022 44th Annual*



- 906 *International Conference of the IEEE Engineering in Medicine & Biology Society (EMBC),*  
907 (IEEE, 2022), pp. 4115–4118.
- 908 15. J. Rossato, *et al.*, I-Spin live: An open-source software based on blind-source separation  
909 for decoding the activity of spinal alpha motor neurons in real-time. *bioRxiv*,  
910 2023.04.14.536933 (2023).
- 911 16. A. K. Clarke, *et al.*, Deep Learning for Robust Decomposition of High-Density Surface EMG  
912 Signals. *IEEE Trans Biomed Eng* **68**, 526–534 (2021).
- 913 17. E. Formento, P. Botros, J. M. Carmena, Skilled independent control of individual motor  
914 units via a non-invasive neuromuscular machine interface. *J Neural Eng* **18** (2021).
- 915 18. C. Chen, S. Ma, X. Sheng, D. Farina, X. Zhu, Adaptive Real-Time Identification of Motor  
916 Unit Discharges From Non-Stationary High-Density Surface Electromyographic Signals.  
917 *IEEE Trans Biomed Eng* **67**, 3501–3509 (2020).
- 918 19. D. Y. Barsakcioglu, M. Bracklein, A. Holobar, D. Farina, Control of Spinal Motoneurons by  
919 Feedback From a Non-Invasive Real-Time Interface. *IEEE Trans Biomed Eng* **68**, 926–935  
920 (2021).
- 921 20. J. Ting, *et al.*, A wearable neural interface for detecting and decoding attempted hand  
922 movements in a person with tetraplegia in *2019 41st Annual International Conference of*  
923 *the IEEE Engineering in Medicine and Biology Society (EMBC)*, (IEEE, 2019), pp. 1930–  
924 1933.
- 925 21. J. E. Ting, *et al.*, Sensing and decoding the neural drive to paralyzed muscles during  
926 attempted movements of a person with tetraplegia using a sleeve array. *J Neurophysiol*  
927 **127**, 2104–2118 (2021).
- 928 22. D. Souza Oliveira, *et al.*, You Will Grasp Again: A Direct Spinal Cord/Computer Interface  
929 with the Spared Motor Neurons Restores the Dexterous Control of the Paralyzed Hand  
930 after Chronic Spinal Cord Injury (2022) <https://doi.org/10.1101/2022.09.09.22279611>.
- 931 23. V. Glaser, A. Holobar, D. Zazula, Real-Time Motor Unit Identification From High-Density  
932 Surface EMG. *IEEE Transactions on Neural Systems and Rehabilitation Engineering* **21**,  
933 949–958 (2013).
- 934 24. D. Y. Barsakcioglu, D. Farina, A real-time surface EMG decomposition system for non-  
935 invasive human-machine interfaces in *2018 IEEE Biomedical Circuits and Systems*  
936 *Conference (BioCAS)*, (IEEE, 2018), pp. 1–4.
- 937 25. C. M. Germer, A. Del Vecchio, F. Negro, D. Farina, L. A. Elias, Neurophysiological  
938 correlates of force control improvement induced by sinusoidal vibrotactile stimulation. *J*  
939 *Neural Eng* **17**, 016043 (2020).
- 940 26. A. Del Vecchio, D. Farina, Interfacing the neural output of the spinal cord: Robust and  
941 reliable longitudinal identification of motor neurons in humans in *Journal of Neural*  
942 *Engineering*, (Institute of Physics Publishing, 2020).

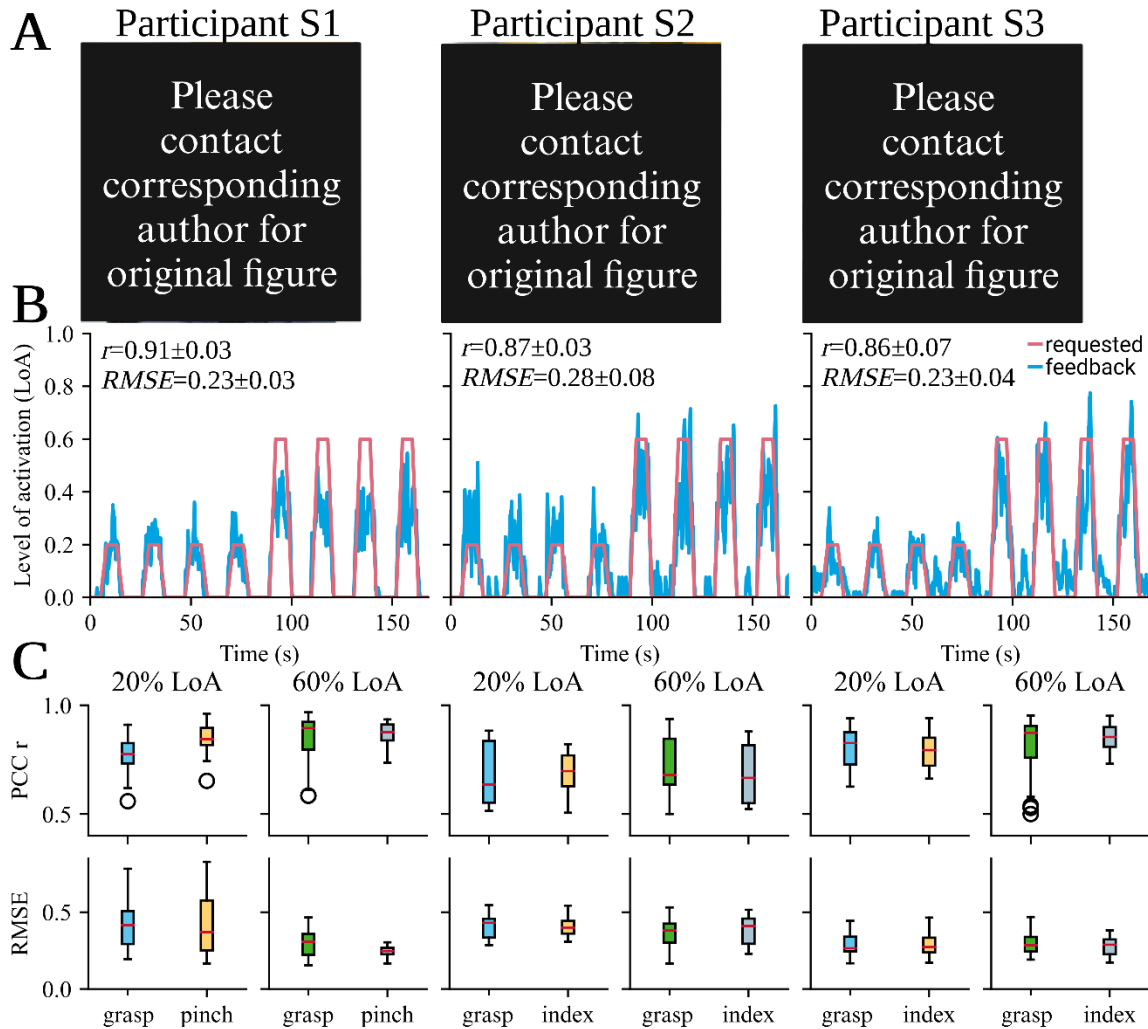
- 943 27. A. Del Vecchio, *et al.*, The increase in muscle force after 4 weeks of strength training is  
944 mediated by adaptations in motor unit recruitment and rate coding. *Journal of*  
945 *Physiology* **597**, 1873–1887 (2019).
- 946  
947

948 **Figures and Tables**  
949



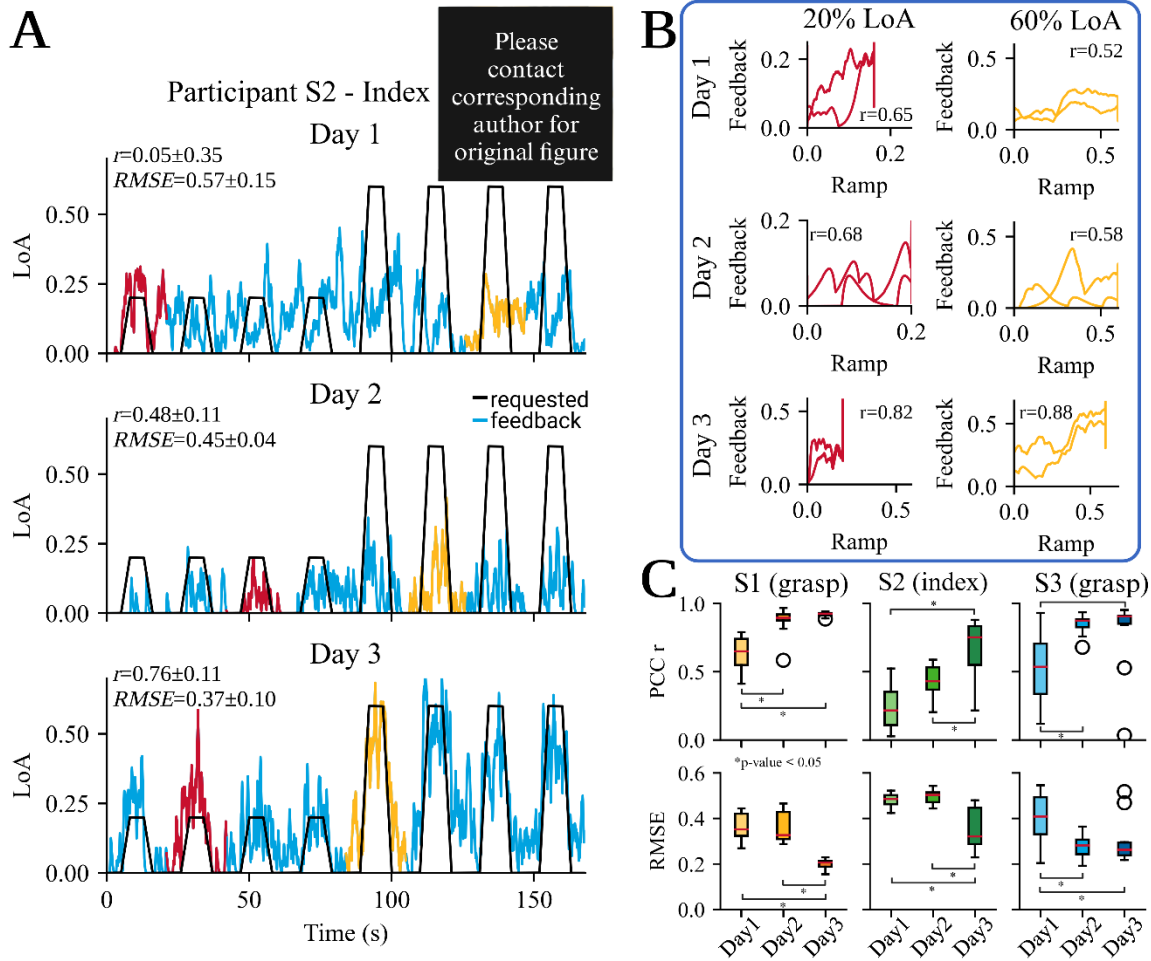
950 **Figure 1.** Overview of the experimental protocol used in individuals with spinal cord injury (SCI).  
951 A) We recorded high-density surface electromyographic (HD-sEMG) signals from the forearms of  
952 participants with SCI by applying two electrode grids with 64 channels each on top of the extensor  
953 digitorum and flexor digitorum superficialis muscles. These signals represent an estimate of the  
954 activity of the spared motor units that controls hand movements. We used a multichannel amplifier  
955 to collect the HD-sEMG signals and stream them to a computer that runs NeurOne. NeurOne  
956 decomposes the streamed HD-sEMG signals into individual motor unit firings. B) NeurOne used in  
957 the study where either offline or online decomposition on the acquired HD-sEMG signals from the  
958 forearm of the participant was performed. By attempting specific hand movements such as power  
959 grasp or pinch, the participants were instructed to follow a trajectory displayed on a screen during  
960 the online session. The neural feedback for the hand movements was calculated by NeurOne and  
961 displayed to the participant through a cursor on a monitor. C) An online session of participant S3,

962 where the participant followed a requested trajectory (red line) by modulating the motor unit activity  
963 (blue line). The participants attempted to control the movement of the paralyzed hand, and the  
964 feedback from NeurOne allowed real-time adjustments of the spared motor commands to achieve  
965 the desired trajectory. D) NeurOne calculates the feedback by convolving the task-related  
966 cumulative motor unit spike train decomposed by NeurOne with a physiological optimized motor  
967 unit twitch model. This approach provides smooth and super-fast feedback that helped the  
968 participants adjusting the movements in real-time.

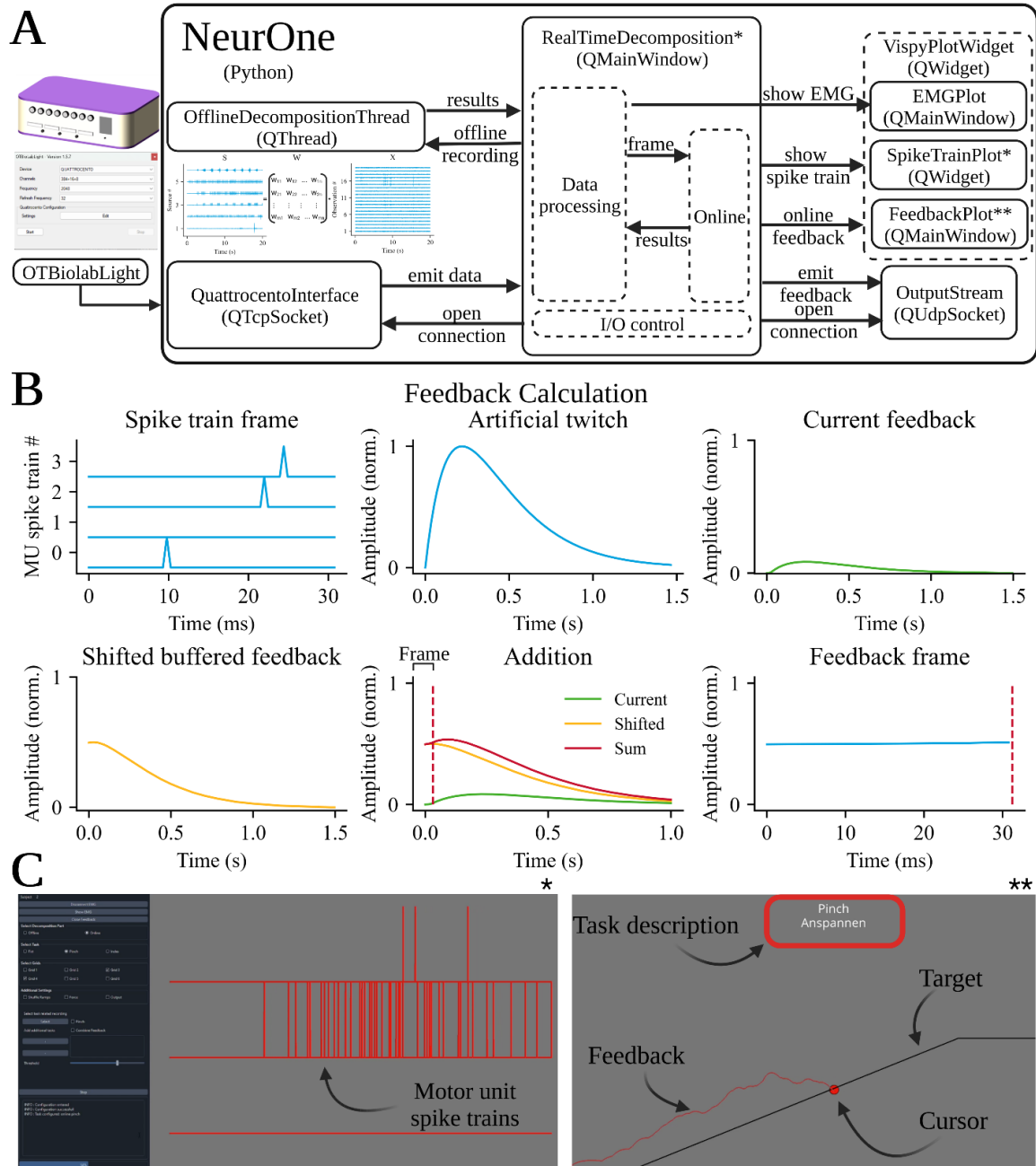


969 **Figure 2.** Performance of the participants in the study. A) The three participants in the study during  
 970 a session. Two electrode grids, each having 64 electrodes are placed on the skin of the forearm of  
 971 the paralyzed hand. After performing a warm-up and recording 20 seconds of high-density surface  
 972 electromyography (HD-sEMG) the online session is performed. B) The best online attempted  
 973 movements throughout all sessions (a total of nine sessions per task spanning over three training  
 974 days) where the participants followed a requested trajectory (red line) consisting of eight ramps by  
 975 their task-related motor unit activity (blue line). The accuracy of the performance is calculated  
 976 through the Pearson correlation coefficient  $r$  and the root-mean-square error  $RMSE$  per activation.  
 977 C) Correlation and error were calculated individually for each ramp/feedback pair throughout the  
 978 first three training sessions for all participants shown for each task and differed between the  
 979 activations of 20% and 60%. Ramp/feedback pairs that had a correlation below  $r < 0.5$  were  
 980 discarded as they were marked as not followed. The correlation  $r$  and error  $RMSE$  demonstrated  
 981 largely consistent patterns between different activation levels and tasks. However, it is noteworthy  
 982 that participant S1 was the only participant showing significant differences between lower and  
 983 higher activations in both metrics.



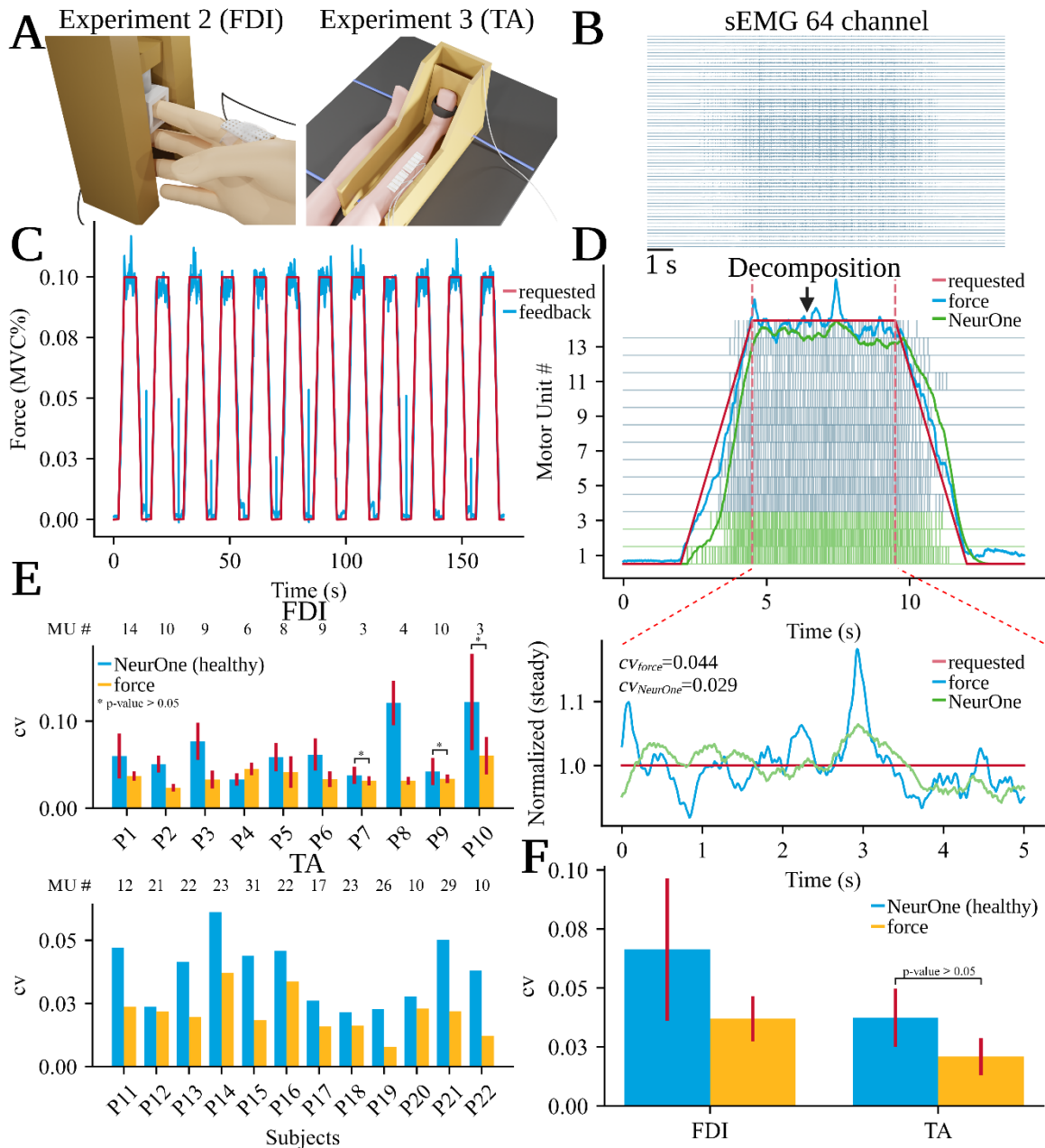


984 **Figure 3.** The effectiveness of the proposed neural feedback system in improving the accuracy of  
 985 tracking a requested trajectory with a cursor. NeurOne was tested on three participants (S1, S2,  
 986 and S3) over three training days spanning between seven days (S2) up to 2 months (S1). A) shows  
 987 the improvement in proportional control of motor unit activity over time for participant S2. On the  
 988 first day of training, no proportional control was observed, as feedback was activated even when  
 989 not requested. However, by the second day, the participant was able to activate motor unit activity  
 990 only when it was requested. On the third day, the participant was able to modulate the feedback  
 991 with high proportionality and low error. B) presents the correlation and error values between the  
 992 best feedback and requested trajectory for each training day for participant S2, as calculated from  
 993 the best correlated feedback/ramp pair in the online recording. The plot demonstrates that the  
 994 correlation improves over the course of the training days. C) Boxplots of the Pearson correlation  
 995 coefficient  $r$  and root-mean-square error  $RMSE$  per activation for each participant at 60% of the  
 996 maximum activation for one task. All participants showed a significant increase in the correlation  $r$   
 997 ( $\Delta r_1=147.6\%$ ,  $p_1=1.33e-6$ ;  $\Delta r_2=275.6\%$ ,  $p_2=8.16e-4$ ;  $\Delta r_3=172.9\%$ ,  $p_3=2.44e-3$  for participants S1,  
 998 S2 and S3 respectively) and a significant decrease in the error from day 1 to day 3  
 999 ( $\Delta RMSE_1=45.6\%$ ,  $p_1=3.54e-5$ ;  $\Delta RMSE_2=25.6\%$ ,  $p_2=0.011$ ;  $\Delta RMSE_3=37.6\%$ ,  $p_3=2.72e-3$   
 1000 for participants S1, S2 and S3 respectively). Participants S1 and S3 achieved consistent accuracy in  
 1001 following the trajectories, as the range in performance at individual ramps decreased ( $\Delta r_1=94.8\%$ ,  
 1002  $\Delta RMSE_1=64.3\%$ ;  $\Delta r_3=98.6\%$ ,  $\Delta RMSE_3=66.9\%$ ) over the training sessions. In contrast, participant  
 1003 S2 showed an increase in the range, but the median values were higher for the correlation and  
 1004 lower for the error on day 3 than on the other days.



1005 **Figure 4.** Overview of NeurOne's software architecture and the feedback calculation process  
 1006 displayed to the participants. A) The software is utilizing the PySide6 Python module and uses a  
 1007 QuattrocentoInterface (based on QTcpSocket) to communicate with the amplification device  
 1008 software *OT Biolab Light*. This data is then sent to the main window of NeurOne, which handles  
 1009 the graphical user interface (GUI), motor unit spike train plots, and data processing. NeurOne can  
 1010 perform either offline or online decomposition of incoming data. The spike trains of all motor units,  
 1011 including those of the main and sub-tasks, are displayed in the main window using the  
 1012 SpikeTrainPlot widget, while the calculated feedback is plotted in a separate FeedbackPlot  
 1013 window (based on QMainWindow), making it possible to display the monitor specifically for the  
 1014 participant in a dual monitor setup. NeurOne can also display the high-density surface  
 1015 electromyographic signals in real-time using the EMGPlot window (based on QMainWindow).  
 1016 NeurOne also provides the functionality of streaming the calculated feedback through an object of  
 1017 the OutputStream class (based on QUdpSocket), which maps the feedback of the selected task

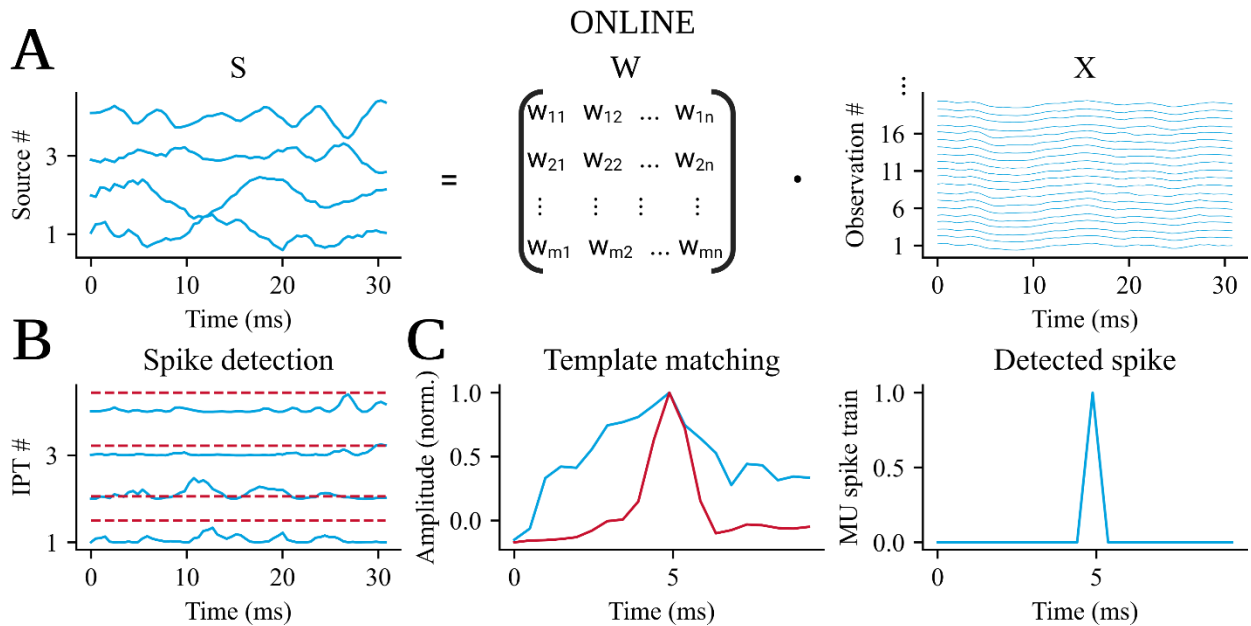
1018 on the involved fingers to control a virtual hand or mechatronic systems. B) The feedback  
1019 calculation that enables fast and smooth feedback for controlling the cursor to track the requested  
1020 trajectory. The identified spike trains of the task-related motor units are summed up into a  
1021 cumulative spike train, which is then convolved with a motor unit twitch model. The induced  
1022 feedback from this frame is then added to the calculated feedback from previous frames. From  
1023 the resulting summed feedback, the first 64 samples, i.e., 31.25 ms (red-dotted line), are taken as  
1024 the feedback frame. The average of the feedback frame is mapped on the cursor. C) Main  
1025 window of NeurOne's GUI that displays the identified motor unit spike trains in real-time (left) and  
1026 the feedback window that is displayed to the participants of the study (right). NeurOne's main  
1027 window allows users to choose tasks, electrode configurations, online and offline parts. In the  
1028 case of the online part, users can select one main task from which the feedback is displayed in  
1029 the feedback window and additional sub-tasks. The real-time decoded motor unit spike trains are  
1030 displayed in the main window, with tasks being colored differently. The feedback window,  
1031 displayed to the participants in the study, provides task instructions and displays the cursor (red  
1032 dot) representing the current feedback frame and its history (red line) while the user is asked to  
1033 follow the requested trajectory (black line) by attempting the pinch task.



1034 **Figure 5.** Procedure used to validate the feedback calculation method of NeurOne. A) Two  
 1035 experiments were conducted that involved placing high-density surface electromyography (HD-  
 1036 sEMG) electrode grids consisting of 64 channels on the first dorsal interosseous (FDI) muscle (left)  
 1037 and the musculus tibialis anterior (TA, rechts) of 23 healthy subjects (10 and 12 in experiment 2  
 1038 and 3 respectively). At the same time, the isometric force produced during index finger abduction  
 1039 (FDI) and ankle dorsiflexion (TA) was measured through a mechanical apparatus. B) A recorded  
 1040 HD-sEMG signal during a ramp contraction of experiment 2 (14 seconds) was analyzed and  
 1041 decomposed into motor unit spike trains. C) The subjects were instructed to follow a specific  
 1042 trajectory with their generated force, consisting of twelve ramps with a target activation level of 10%  
 1043 of maximum voluntary contraction (MVC). The requested trajectory is displayed with the red line  
 1044 and the force feedback measured with the blue line (displayed for experiment 2). D) The cumulative  
 1045 spike train of the three motor units (green) from the recorded HD-sEMG signal during a ramp  
 1046 contraction of the index finger abduction task were used in the feedback calculation approach of  
 1047 NeurOne. Additionally, the requested trajectory (red), the force signal (blue), and the feedback

1048 calculated by NeurOne (green) are displayed. Four seconds of the plateau part of the ramp  
1049 (between the vertical dotted red lines) were extracted for each signal and experiment and  
1050 normalized on its mean. Furthermore, the coefficient of variation  $cv$  was calculated for the  
1051 presented ramp plateau. E) The mean and standard deviation of the coefficient of variation  $cv$  were  
1052 calculated for each participant of experiment 2 (FDI, P1-10) and 3 (TA, P11-22) across all ramps.  
1053 The coefficient of variation  $cv$  was displayed for the output of NeurOne's feedback calculation  
1054 method (blue bars) and the recorded force signals (yellow bars) for the healthy subjects. F) Average  
1055 coefficient of correlation  $cv$  across all participants for experiment 2 and 3.





1056 **Figure 6.** This figure depicts the online decomposition method that is utilized in our software,  
1057 NeurOne. The process involves three steps. A) First, the source signals are identified in real-time  
1058 by applying the separation matrix  $W$ , which was discovered in the offline stage on the extended  
1059 and centered high-density surface electromyographic (HD-sEMG) signals of the current frame. B)  
1060 Next, a spike detection technique is applied to the identified sources. This method detects the  
1061 peak in the innervation pulse trains (IPTs), which are the squared source signals of this frame. If  
1062 the peak of the IPT is greater than 10 times the noise level, it is designated as a possible spike.  
1063 C) Finally, template matching is conducted to verify whether the possible spike is a motor unit  
1064 firing or not. To achieve this, a window is implemented around this possible spike in the source  
1065 signal and then correlated with the motor unit action potential that was identified in the offline  
1066 stage. If the correlation coefficient  $r_{\text{threshold}} > 0.60$ , the spike is identified as a motor unit firing.

1067 **Table 1.** Characteristics of recruited participants in the study

Subject	Age range (years)	Gender	Injury level	AIS	Sensory level*	Wrist movement	Time since injury (years)
S1	31-35	M	C5	B	C5	yes	9.1
S2	36-40	F	C5	A	C5	yes	24.2
S3	56-60	M	C5	A	T3	no	6.9

1068 \* The sensory level corresponds to lowest level with normal sensory function.